SEARCH FOR $\psi(2S) \to \Lambda\bar{\Lambda}K_S^0$

ABRAR AHMAD ZAFAR

Centre for High Energy Physics
University of the Punjab
Lahore, PAKISTAN

February, 2010

SEARCH FOR $\psi(2S) \to \Lambda\overline{\Lambda}K_S^0$

Abrar Ahmad Zafar

Submitted in Partial Fulfillment of the Requirements for the Degree of

DOCTOR OF PHILOSOPHY

at

Centre for High Energy Physics

University of the Punjab

Lahore, PAKISTAN

February, 2010

Dedicated to

My Parents, Wife and Children

CERTIFICATE

It is certified that I have read this dissertation and that, in my opinion, it is fully adequate in scope and quality for the degree of Doctor of Philosophy.

Prof. Shan Jin
(Supervisor)

Prof. Dr. Haris Rashid
(Supervisor)

Submitted through

Prof. Dr. Haris Rashid
(Supervisor & Director)

DECLARATION

This work represents the effort of the members of the BES collaboration at the Institute of High Energy Physics, Beijing, CHINA. I claim the credit for the analysis and final results presented in this thesis which are entirely my own and were compiled as a member of the Charmonium Group.

This thesis which is being submitted for the award of degree of Ph.D. in the University of the Punjab does not contain any material which has been submitted for the award of any other degree or diploma in any university and, to the best of my knowledge and belief, neither contain any material published or written by another person, except when due reference is made to the source in the text of the thesis. If any reference is found missing in this thesis that would completely be unintentional and I do not have any pretension to own the credit for that.

Abrar Ahmad Zafar

SEARCH FOR $\psi(2S)$ DECAYS INTO $\Lambda\ \bar{\Lambda}\ K_S^0$

By

Abrar Ahmad Zafar

SUBMITTED IN PARTIAL FULFILLMENT OF THE

REQUIREMENTS FOR THE DEGREE OF

DOCTOR OF PHILOSOPHY

AT

UNIVERSITY OF THE PUNJAB

LAHORE, PAKISTAN

FEBRUARY 2010

Table of Contents

List of Tables

List of Figures

List of Papers

- Analysis Memo based upon *Search for* $\Psi(2S) \to \Lambda\bar{\Lambda}K^0_s$, has been finalized by BES Collaboration and is being submitted for publication, 2009.

- "GEANT4: Applications in High Energy Physics", AIP Conf. Proc.,Volume 888, February 14, 2007, pp. 301-304.

Abstract

Using 14 million $\psi(2S)$ decay events registered by Beijing Spectrometer II commonly known as BESII at Beijing Electron Positron Collider (BEPC), we have performed detailed study of $\psi(2S) \to \Lambda\bar{\Lambda}K_s^0$ (a strangeness and isospin violating process), to look for any hint beyond the 'Standard Model'. Finding no obvious signal, we report, first time, an upper limit of 9.3×10^{-5} at 90% confidence level, for the branching fraction.

Acknowledgements

All praise be to Almighty Allah who provided me strength and courage to complete this research work. I offer my humblest and sincerest words to the Holy Prophet (pease be upon him, who is forever a torch of guidance and knowledge for humanity). I feel great pleasure in expressing my sincerest and warmest thanks to my supervisors, Professor Dr. Shan Jin, Experimental Physics Centre, Institute of High Energy Physics (IHEP), Beijing China and Professor Dr. Haris Rashid, Centre for High Energy Physics, University of the Punjab Lahore. They have been very helpful, most generous, dedicated and encouraging throughout this research work. I owe special thanks to Professor Shan Jin for his patient instructions and kind guidance throughout my stay at IHEP. I am also indebted to all the members of BES collaboration. I thank Mr. Wang zhiyong, Miss Yamping, Mrs. Li Xiaoling and Charmoniuam group leader Yuan for their support and suggestions.

I am out of words in expressing my sincere gratitude to Professor Haris Rashid. Without his support and encouragement, completion of this work would not have been possible. I am equally thankful to Dr. Qadeer Afzal Malik for his sincere efforts

in making arrangements at IHEP, China. I am immensely thankful to Mr. Talab Hussain for his pleasant and enjoyable company throughout the study. Thanks are also due to my friends and colleagues, Mr. Tariq Mahmood, Mr. Anjum Javed, Dr. Maqsood Ahmad, Mr. Rashid Ahmad, Dr. Alam Saeed, Mr. Ayub Faradi for their encouragement throughout the period.

Finally, I take this golden opportunity to offer my gratitude to my loving mother and father who sent me on the path towards intellectual pursuit. I am also thankful to my brother and sisters who remembered me in their prayers. I also owe a very special thanks to my wife, who always encouraged me throughout the span of my studies. My children Ibrahim Zafar and Khadeeja Zafar equally share a special credit for facing hardships during my period of absence.

I am also thankful to Higher Education Commission of Pakistan and University of the Punjab for their continued support throughout my Ph.D studies.

(Abrar Ahmad Zafar)

Chapter 1

Introduction

High Energy Physics deals with the study of fundamental particles and their interactions. In this regard, both the theoretical as well as experimental approaches are used [1]. On the theoretical side, 'Standard Model' of Particle Physics is the best framework. It provides mathematical tools to investigate the electroweak and strong interactions among fundamental particles [2]. In the electroweak sector, this theory is highly successful. On the other side, many high energy physics experiments use the accelerator and detector technology to create environment necessary for the study of fundamental physics. The experimental setup might involve fixed target or colliding beams. BESII is one of the leading high energy physics experiments. In this experiment, electron positron beams were collided at 2-5 GeV energy range. In addition to other physics agenda, large samples of charmonium states (containing

charm anticharm pair): J/ψ, $\psi(2S)$ and $\psi(3S)$ were produced. The $\psi(2S)$ sample consists of about 14 million events. The decay dynamics of charmonium states like $\psi(2S)$ can be investigated to test the laws of symmetries claimed by the 'Standard Model'. These laws include conservation of different quantum numbers such as baryonness, strangeness, charmness, bottomness, isospin, etc. As far as law of conservation of baryon number is concerned, until now, it is followed by electroweak as well as strong reactions. However, law of 'conservation of strangeness' is not obeyed in weak interactions. According to Quantum Chromodynamics (QCD), $\psi(2S)$ decays predominantly through electromagnetic and hadronic transitions. There is also large probability of strong decays of $\psi(2S)$, in which its charm anticharm ($c\bar{c}$) pair first annihilates into three gluons or one photon. Then the gluons or the photon materializes into hadronic states (stable or unstable) ([3], [4], [5]). There is no QCD prediction about the strangeness violating decay of $\psi(2S)$, meaning such decay process has zero chances. Looking for strangeness violating decay of $\psi(2S)$ is actually looking beyond the 'Standard Model'. In order to test the 'Standard Model' for strangeness violation in $\psi(2S)$ primary decays, we have performed a detailed study of $\psi(2S) \to \Lambda\bar{\Lambda}K_s^0$. Our study reveals that, as predicted by the 'Standard Model', both the isospin as well as strangeness are violated from the origin. Only isospin violating process $J/\psi,\ \psi(2S) \to \Lambda\bar{\Lambda}\pi^0$ has been studied by BES and DM2 (Magnetic Detector 2) Collaborations ([6], [7], [8]). However, no study of strangness violation exists in literature for our decay process. At BESI and BESII ([6], [7]), the study of

$J/\psi \to \Lambda\bar{\Lambda}\pi^0$ has been reported with a branching fraction and an upper limit of the branching fraction, respectively. Our study confirms isospin and strangness violation in $\psi(2S) \to \Lambda\bar{\Lambda}K_s^0$, with an upper limit of 9.3×10^{-5} at 90% confidence level through Bayesian approach, for branching fraction.

Chapter 2

Fundamental Concepts

2.1 Brief History

Scientists have always been attempting to discover the internal structure of matter and the forces which bind the matter together. At first, atom was considered as the fundamental building block of matter. As the research proceeded it was found that atom itself had an internal structure. The existence of electron was confirmed in 1897 by J.J. Thomson in the study of cathode rays ([9], [10]). According to his 'plum pudding model' an atom consisted of electrons dispersed in a rather homogeneous positive sphere. The atomic structure was discovered by Rutherford in an experiment of protons striking piece of gold foil. He concluded that electrons which are negatively charged particles, revolve around positively charged nucleus. Later on, proton and neutron, were discovered forming nucleus. In 1930's, Pauli gave the idea of neutrinos,

to account for the energy and momentum missing in nuclear β decay ([3], [10]). Later studies indicated that even protons and neutrons themselves have substructure. Efforts to discover and understand the fundamental particles went on throughout the last century. In this persuit, we now know that the basic constituents of matter and their properties can be well studied in the framework of 'Standard Model'. High energy physics experiments are looking to confirm the predictions of the Standard Model, and beyond. Similar efforts are ongoing at BEPC and our work focuses on an important aspect of the same in the domain of "strong interactions". The following section provides a brief description of some important aspects of the Standard Model which are related to our work.

2.2 The Standard Model

'Standard Model' is a set of quantum field theories that provides a theoretical framework to study fundamental particles and their interactions. The fundamental particles are of two types: quarks and leptons. Each of the quarks and leptons has corresponding antiparticle called antiquark and antilepton, respectively([2], [3]). There are four known interactions: electromagnetic, weak, strong and gravitational. The gravitational force is negligible at quantum level as compared to other three types. Thus we are left with only three forces working among the fundamental building blocks of matter. Leptons interact through only electromagnetic and weak forces. While

quarks due to color property, interact in all the three ways. Electromagnetic interaction takes place among electrically charged particles, through exchange of photons (γ). The weak force is mediated by three types of bosons: W^+, W^- and Z^0. The strong force is mediated via exchange of gluons. Electromagnetic and weak forces have been unified into the electroweak force which is studied in the framework of electroweak theory. Efforts to explore the properties of strongly interacting particles within the Standard Model are ongoing.

Main properties of the fundamental forces and their gauge bosons as described in reference 4 is reproduced in Table 2.1.

Table 2.1: The Boson Mediator[4]

Force	Mediator	Mass (GeV/c^2)	Range (fm)	Spin/Parity
Strong	Gluon (g)	0	~ 1	1^-
Electromagnetic	Photon γ	0	Infinite	1^-
Weak	Z^0	91.186 ± 0.0021	$\sim 10^{-3}$	1^+
	$W^{\pm}$	80.403 ± 0.029	$\sim 10^{-3}$	1^-

In the following sections, we review the basic concepts of quarks and leptons, with a special focus on the bound states of quarks and/or antiquarks called hadrons([3], [5], [9], [11], [12]).

2.3 The Quark Model

Initially, the purpose of quarks was just to explain flavor patterns of particle masses. There was no postulate that quarks are actual physical objects. Later on, theoretical and experimental investigations indicated that quarks are real physical objects, although there is no direct experimental evidence of these entities [13]. Currently, according to the quark model, there are six quarks and six leptons, each having spin 1/2. By convention quarks are assigned positive parity and antiquarks a negative parity. In addition, each quark has baryon number 1/3 and antiquark $-1/3$. The six quark types (flavors) are: up, down, strange, charm, bottom and top. The lepton types include: electron (e), electron neutrino (ν_e), muon (μ), muon neutrino (ν_μ), tau (τ) and tau neutrino (ν_τ). The properties of quarks and leptons as described in Particle data booklet [14] are listed in Tables 2.2. and 2.3. The additive quantum numbers of quarks are associated with their electric charge through the following generalized Gell-Mann-Nishijima formula([14], [15], [16], [17]):

$$Q = I_3 + \frac{B + S + C + B_f + T}{2}, \tag{2.3.1}$$

where B the baryon number, Q is the electric charge, S the strangeness, C the charmness, T the topness, B_f the bottomness and I_3 the third component of isospin of any quark type.

In the minimal quark model, baryons (antibaryons) are composed of three quarks (antiquarks) and mesons are made up of quark antiquark pair. Therefore each baryon

Table 2.2: Fundamental Fermions [14]

Particle	Mass (GeV/c^2)	Electric Charge
Quarks		
u	$\sim 0.0015 - 0.004$	+2/3
d	$\sim 0.004 - 0.008$	-1/3
c	$\sim 1.15 - 1.35$	+2/3
s	$\sim 0.08 - 0.13$	-1/3
t	174.3	+2/3
b	$\sim 4.1 - 4.3$	-1/3
Leptons		
e	5.1×10^{-4}	-1
ν_e		0
μ	0.11	-1
ν_μ		0
τ	1.8	-1
ν_τ		0

Table 2.3: "The additive quantum numbers of the quarks". [14]

Property Quark	d	u	s	c	b	t
Q (charge)	$-\frac{1}{3}$	$\frac{2}{3}$	$-\frac{1}{3}$	$\frac{2}{3}$	$-\frac{1}{3}$	$\frac{2}{3}$
I (Isospin)	$\frac{1}{2}$	$\frac{1}{2}$	0	0	0	0
I_3 (3rd comp.)	$-\frac{1}{2}$	$\frac{1}{2}$	0	0	0	0
S (Strangeness)	0	0	-1	0	0	0
C (Charm)	0	0	0	+1	0	0
B (Bottomness)	0	0	0	0	+1	0
T (Topness)	0	0	0	0	0	+1

(such as proton (p), neutron (n), Λ, Δ, Σ, Ξ, Ω,...) has baryon number +1. In the same way, the baryon number for each antibaryon (such as antiproton ($\bar{p}$),antineutron ($\bar{n}$), $\bar{\Lambda}$, $\bar{\Delta}$, $\bar{\Sigma}$, $\bar{\Xi}$, $\bar{\Omega}$, ...) is -1. The baryon number for each meson is zero. All of the additive quantum numbers are conserved in strong interactions. The strangeness is an exceptional additive quantum number helpful in distinguishing weak processes from strong and electromagnetic reactions, because its conservation is only violated in weak interactions. By convention, each strange quark is assigned a strangeness of -1 and antistrange quark +1 ([15], [16], [17], [18]).

When extended to SU(4) or SU(5), the quark model can include all quark-antiquark combinations allowed by QCD ([13], [18], [19], [20]) , i.e. all colour neutral configurations: tetraquarks $(qq)(\bar{q}\bar{q})$, meson-molecules $(q\bar{q})(q\bar{q})$ and pentaquarks $(q\bar{q}qqq)$. However, Glueballs (gg) or hybrids $(q\bar{q}g)$ are not included in the quark model framework, since there are no explicit gluons in the quark model.

The decay process which we intend to analyze in this work, namely $\psi(2S) \to \Lambda\bar{\Lambda}K_s^0$, involves both the baryons as well as mesons in the primary, secondary and tertiary level decay products. We will therefore focus on the their formation from quark/antiquark constituents in the following subsection. The mesons and baryons are grouped depending upon their similar properties such as j^{PC}, where j, P and C represent total angular momentum, parity and charge conjugation, respectively.

2.3.1 Meson Multiplets

As described earlier, meson is a bound state of quark antiquark pair, characteristics of which (such as parity, C-parity, G-parity, spin j etc), are described by the properties of its constituents. Parity of a meson is obtained through the following relation [21]:

$$P = (-1)^{l+1}$$

C-parity and G-parity of a meson are obtained using the following relations:

$$C = (-1)^{l+s}$$

and

$$G = (-1)^{I+l+s}. \tag{2.3.2}$$

The spin quantum number j of a meson satisfies the following relation:

$$|l - s| < j < |l + s|$$

where l is the angular momentum quantum number and s is the spin angular momentum quantum number of meson. In case of antiparallel quark and antiquark spins; s = 0 and for parallel quark and antiquark spins; s = 1. The angular momentum number l can have values 0, 1, 2 and so on. The value $l = 0$ corresponds to ground state mesons. Mesons are grouped according to their j^{PC} values. The groups thus obtained are called meson multiplets [14].

Three quark antiquark flavors (u, d and s) make up nine $q\bar{q}$ combinations for light

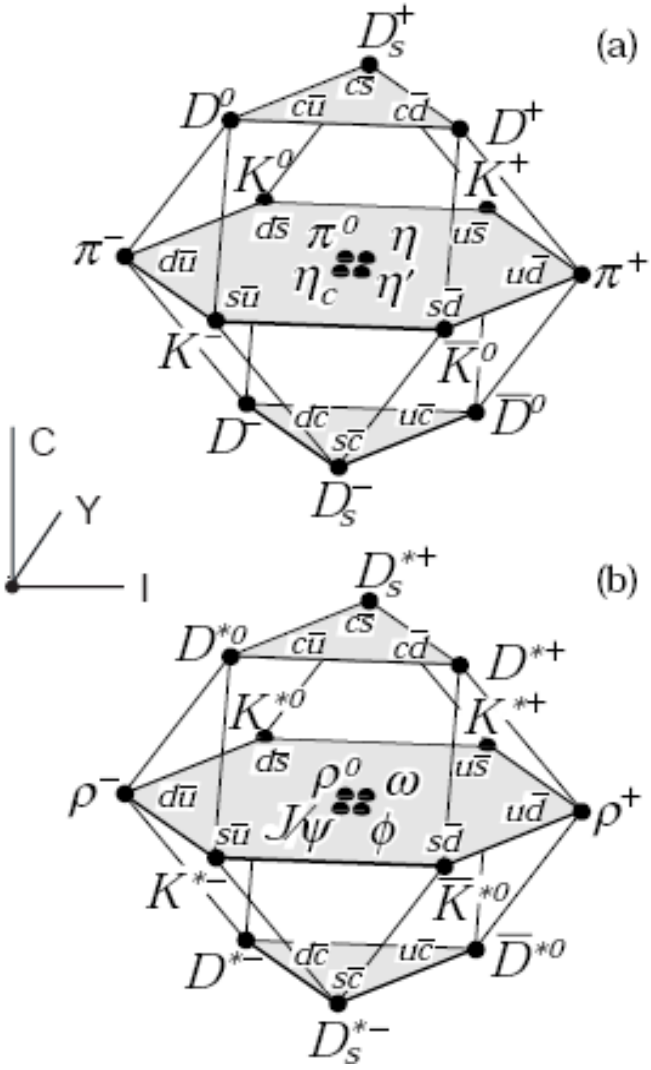

Figure 2.1: "SU(4) weight diagram showing the 16-plets for the pseudoscalar" (a) "and vector mesons (b) made of the u, d, s and c quarks as a function of isospin I, charm C and hypercharge $Y = S + B - C/3$. The nonets of light mesons occupy the central planes to which the $c\bar{c}$ states have been added" [14].

as well excited mesons, giving an octet and a singlet [14]:

$$3 \otimes \bar{3} = 8 \oplus 1$$

If c quark is also included, sixteen meson states are obtained which form a 15-plet and a singlet [14]:

$$4 \otimes \bar{4} = 15 \oplus 1$$

The ground state mesons include both the pseudoscalar as well vector mesons. The nonets of these mesons make up the central plane of Fig.2.1 (a) and Fig 2.1 (b) [14]. The nonent of Fig. 2.1 (a) includes the pseudo scalar mesons of our decay channel i.e., K_s^0, π^- and π^+ whereas that of Fig. 2.1 (b) includes the vector meson J/ψ. The vector meson resonance involved in our decay process $\psi(2S)$ is the first excited state of the J/ψ meson.

2.3.2 Baryon Multiplets

In minimal quark model, baryon is a bound state of three quarks, with fermionic nature. Baryon spin (j) is sum of its orbital angular momentum (l) and total spin (s) of quark constituents. For $l = 0$, with two quarks aligned and one anti-aligned, the spin is 1/2, and with all quarks aligned, spin is 3/2. For spin 1/2, an octet of baryons is allowed, whereas for spin 3/2, a decuplet of baryons is formed. When charm quark is included among three light quarks, a 20-plet for each of the baryons with spin 1/2 and spin 3/2, is obtained. These 20-plets of baryons, plotted with respect to their hypercharge, third component of isospin and charmness, are shown in Fig. 2.2. The

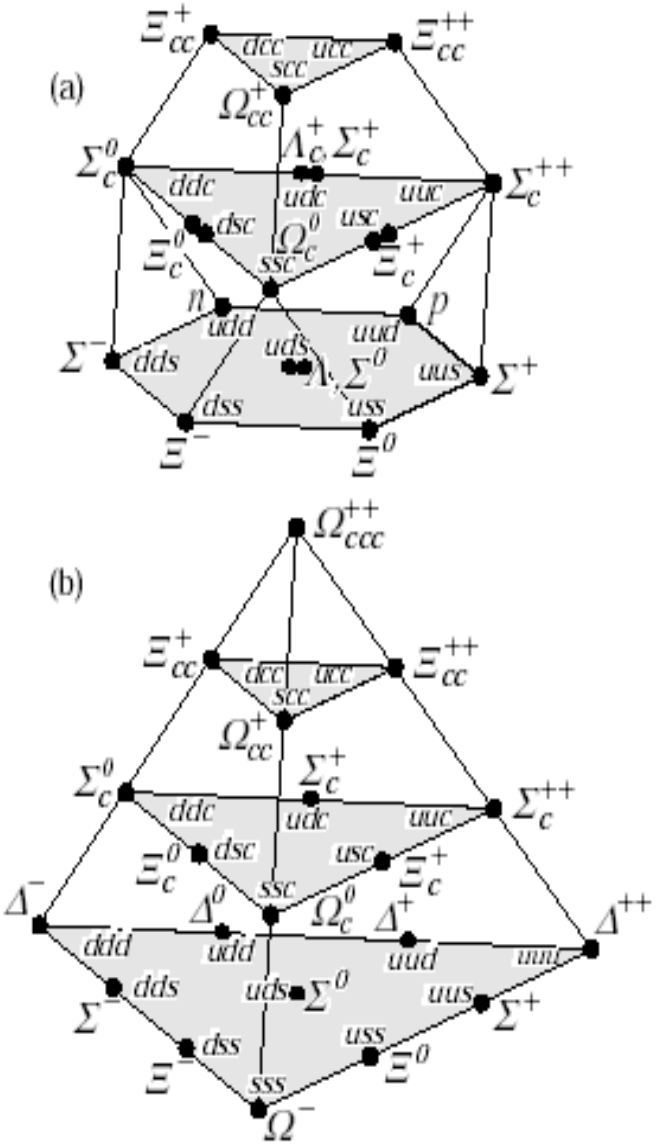

Figure 2.2: "SU(4) multiplets of baryons made of u, d, s, and c quarks". (a) "The 20-plet with an SU(3) octet. (b) The 20-plet with an SU(3) decuplet". [14].

octet and the decuplet allowed for light quarks, are clearly found as lowest planes in Fig. 2.2 (a) and Fig. 2.2 (b) ([14], [21]). Fig 2.2 (a) also includes the baryons of our decay process: lambda (Λ) and proton (p).

The properties of unstable hadrons such as $\psi(2S)$ can be studied through analysis of their final decay products. As described above, our analysis uses 14 million $\psi(2S)$ decay events recorded by BESII experiment. Before going to the details of our analysis, first of all, we will describe the BESII experimental setup in the following chapter.

Chapter 3

Experimental Setup

3.1 Beijing Electron Positron Collider (BEPC)

[1]The Beijing Electron Positron Collider (BEPC) ([22], [23]) was constructed on the grounds of Institute of High Energy Physics (IHEP), Beijing, China, from 1984 to 1988. Its purpose was to produce electron positron beams for collisions at the center of mass energies in the range: (2-5) GeV.

From 1993 to 1997, the collider (and detector) was upgraded [23] to BEPCI (and BESII), the focus of our study. The running parameters of BEPCI are listed in Table 3.1 [25]. An overview of different parts of BEPC is shown in Fig. 3.1.

The details about different parts of BEPC can be found at: "*http://www.ihep.ac.cn/english/E-Bepc/index.htm*". The upgraded setup was used to record data

[1]Material presented in this chapter has been taken from scholarly work whose references are given. Author does not have any intention to own any material reported without references.

Table 3.1: The running parameters of BEPC [25]

Parameter	**Operation values**
Operation momentum, $Pe^{\pm}$	1.0-2.5 GeV/c
Energy spread ΔE/E	2.64×10^{-4}
Circumference	240.4 m
Bunch number	1 e^- and 1 e^+
Bunch length	$\sim 5\ cm$
Beam lifetime	6-8 h
Luminosity at 1.89 GeV	$10^{31}\ cm^{-2}s^{-1}$

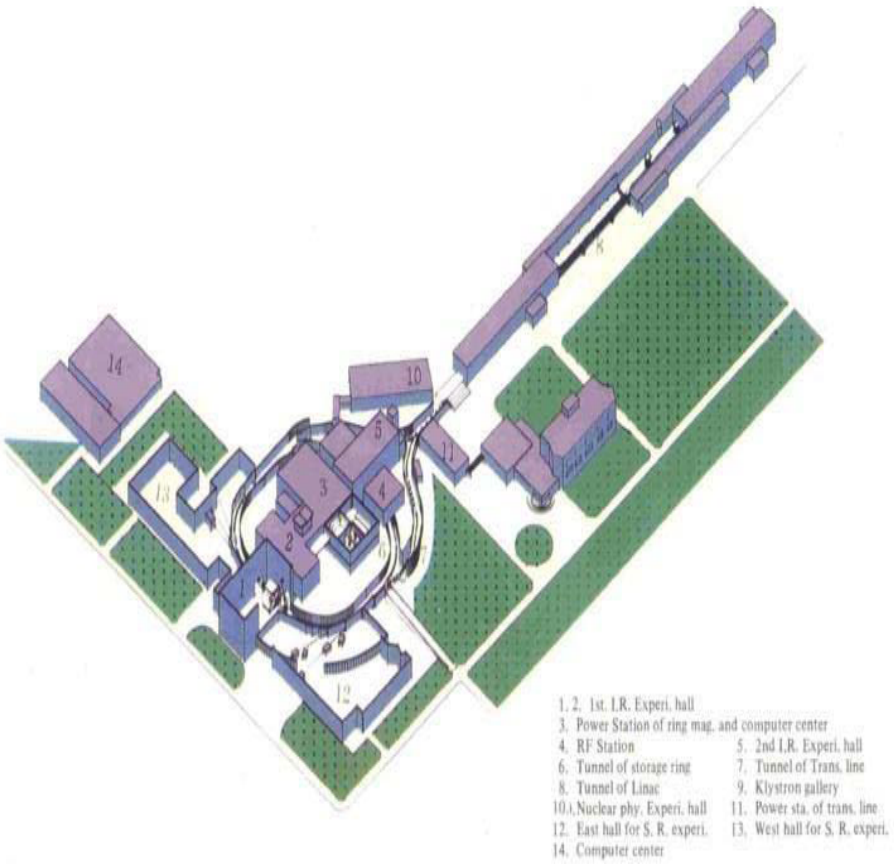

Figure 3.1: Schematic view of BEPC [26].

from 1997 to 2002. The data recorded for $\psi(2S)$ events [27] comprise of 14 million registered from 2001 to 2002, at cm energy of 3.686 GeV. This data has been used for studying many electroweak and strong processes [28]. The current study has also been carried out using this data. Keeping in view the importance of the detector setup used to record data, it is necessary to describe its functional parts. Therefore, the functionalities of different parts of BESII detector are described in the following sections.

3.2 BESII Detector

It is a solenoidal detector, consisting of several parts for measuring specific information about particles of data events produced at its middle from electron positron collisions ([23], [29], [30]).

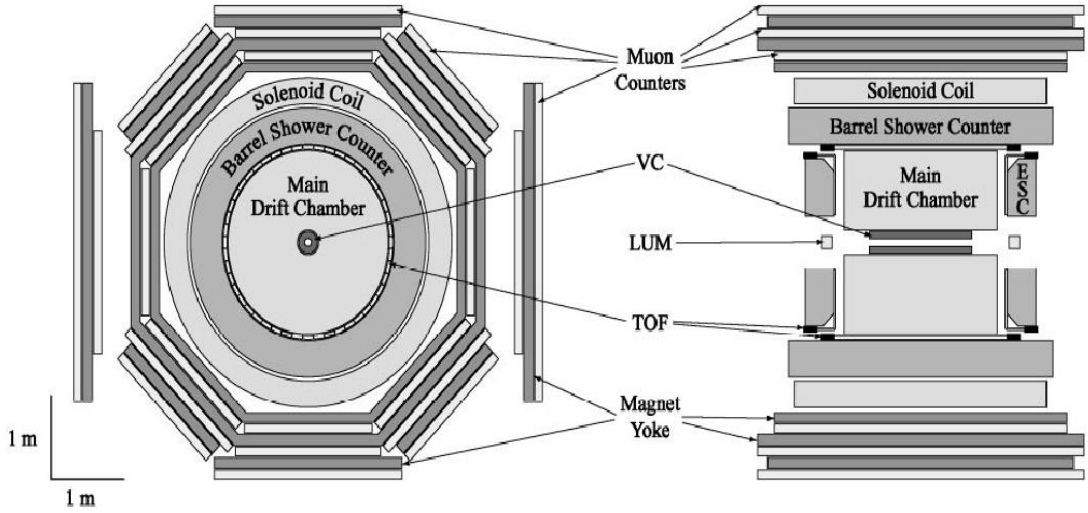

Figure 3.2: End and side views of the BESII detector ([30], [31])

When data events are produced, their final state particles move outwards traversing through different parts of the BESII detector. These parts include a vertex chamber (VC), a main drift chamber (MDC), time-of-flight (TOF) system, electromagnetic shower counters (ESC) and the muon counters. The position and order of the detector parts can be seen in its side and end views, as shown in Fig. 3.2. Main detector parts have been explained elegantly by Mr. Taiki Yamamura in his PhD thesis [31]. In the following subsections we describe their main aspects.

3.2.1 Vertex Chamber

The VC was configured around the Beryllium beam pipe of diameter 9.8 cm and thickness of 1.2 mm. It works with MDC to improve the acceptance and momentum resolution. When used with TOF system for triggering events, it reduces cosmic ray background. Its quarter section is shown in Fig. 3.3 ([29], [32]). From this figure it can be seen that there are 12 layers of straw-tube chambers of two types: axial and stereo chambers. The inner 4 layers and outer 4 layers are of axial type whereas the middle 4 layers are stereo type. The stereo type layers have tilting angle of ± 3 degrees with the beam axis. Each straw-tube chamber has position resolutions of (73.4 ± 8.4) μm and 90 μm, for cosmic ray and colliding beam data, respectively [31].

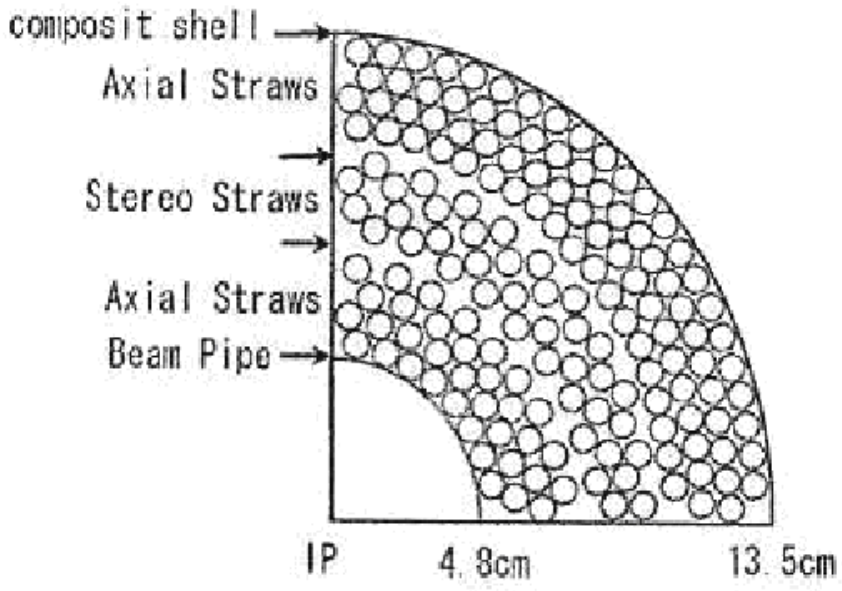

Figure 3.3: End view of quarter section of the Vertex Chamber ([29],[31])

3.2.2 Main Drift Chamber

The MDC ([29], [31], [33]) is a concentric cylindrical chamber surrounding the VC. It is a large tracking detector, the heart of BESII. In addition to the trigger information of the events, it also measures the trajectory, momenta and energy loss (dE/dx) of the charge tracks. The structure of MDC is shown in Fig. 3.4.

It had a 40 layer open cell geometry covering 85% of the solid angle. It had one single gas-filled volume with 3216 sense-wires for readout and 19720 field-wires for field shaping. Its principle is similar to the straw-tube chamber: a charged particle passes through it and creates ionization along its way. Being in an electric field, the ionization electrons are collected and amplified on the sense wires.

Consequently a signal is read out as an electric pulse at the end of these wires. Inside

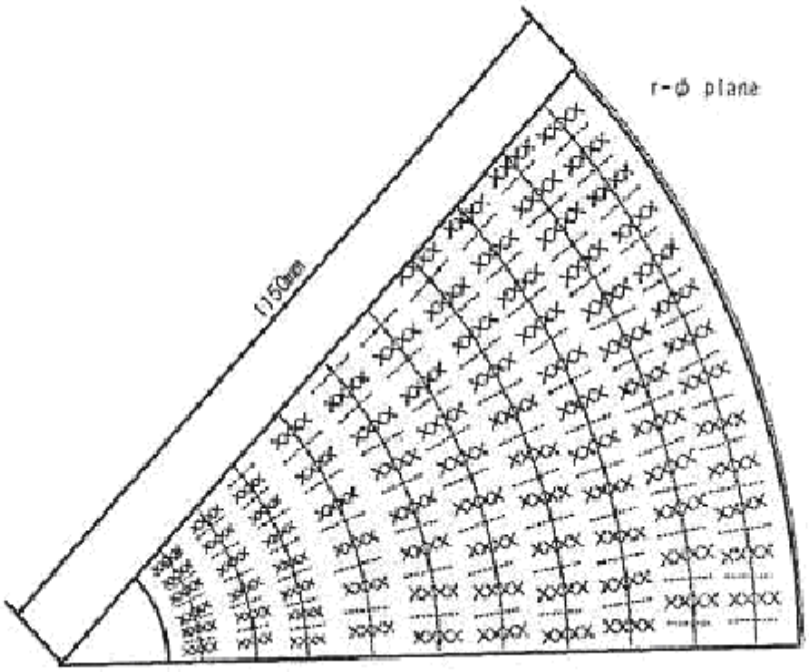

Figure 3.4: Cell structure of MDC ([29],[31]

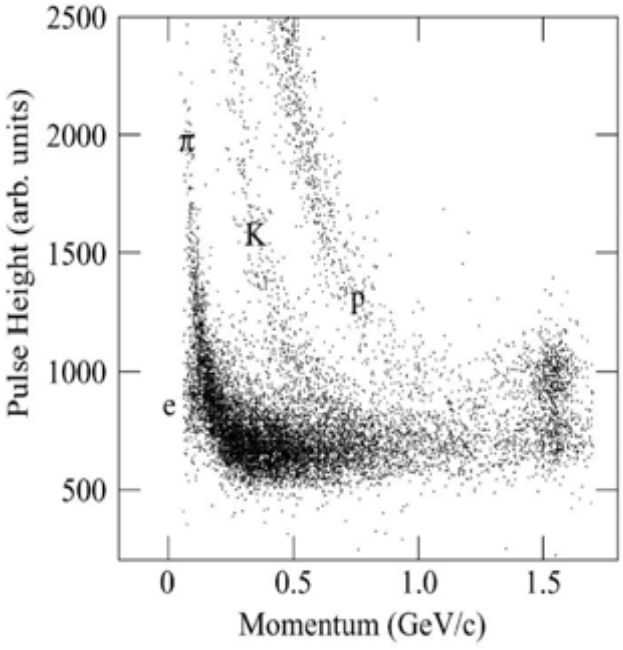

Figure 3.5: The dE/dx resolution of BESII detector [30].

a 0.4 T magnetic field, the momentum resolution of BESII detector was $\sigma_p/p = 1.78\%\sqrt{1+p^2}$ where p is in GeV/c. In addition to $r\phi$ -coordinate information, the MDC also provides dE/dx information used in particle identification. The dE/dx value depends upon the particle momentum, thus being unique for each particle type (Fig. 3.5). The greater the energy loss, the more ionizations occur, resulting in larger electric pulse.

3.2.3 Time of Flight Counter

After VC and MDC, comes the TOF system at a radius of 1.15 m. It is divided into two parts: the Barrel-TOF and Endcap-TOF. It has 48 scintillation counters to signal as charged particle hits its counters [29].

To supplement particle identification, the mass of the particle is deduced by using flight time from the interaction point to the TOF and the momentum information. The time resolution for Bhabha events [34] ($e^+e^- \to e^+e^-$) was 180 ps and for hadrons 200 ps, enough for a reasonable separation of charged kaons, pions and protons below 1 GeV/c (Fig. 3.6) [31].

3.2.4 Shower Counter

The shower counter consists of both the barrel-shower-counter (BSC) and end-cap-shower-counter (ESC) ([35], [36]). The BSC lies between barrel TOF and the magnetic coil whereas ESC was between end-cap TOF and magnet yoke. It covered 80% and

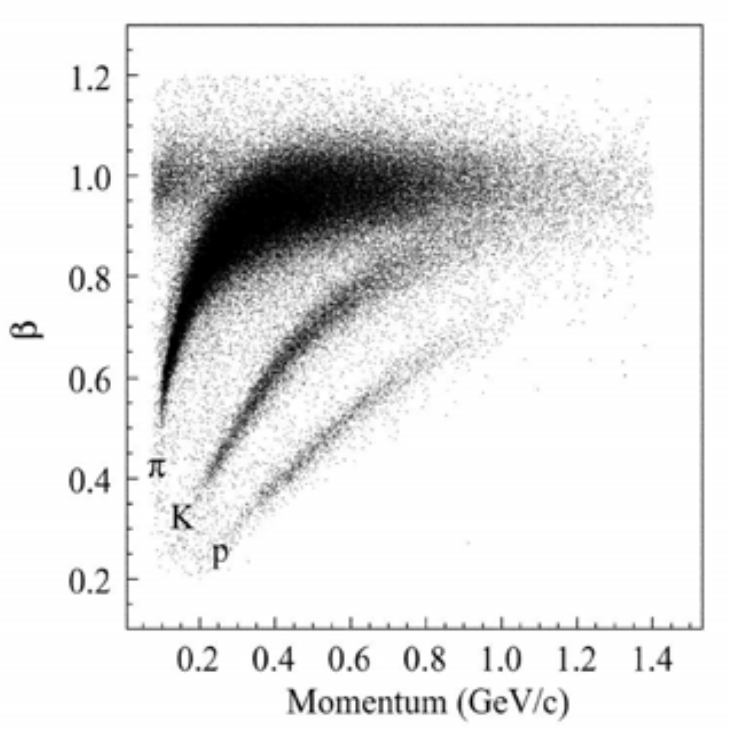

Figure 3.6: Time of flight resolution at BESII [30]

13% of the solid angle for BSC and ESC, respectively. Fig. 3.7 and Fig. 3.8 show schematic views of BSC and ESC, respectively [31].

The BSC consists of 24 layers of self-quenching streamer mode (SQS) tubes interleaved with 24 layers of lead absorber (0.5 radiation length each). The SQS-tubes were mounted axially with readout on wires. The position along the z-axis was determined by charge-division, i.e. by comparing the signal strength from both ends of the wire. The BSC was used to measure energies of photons and electrons over 80% of the solid angle. The ESC consisted of 24 layers of self-quenching streamer (SQS), interleaved with 23 layers of lead sheet [31]. It was used to measure energies of electrons and photons over 13% of the solid angle.

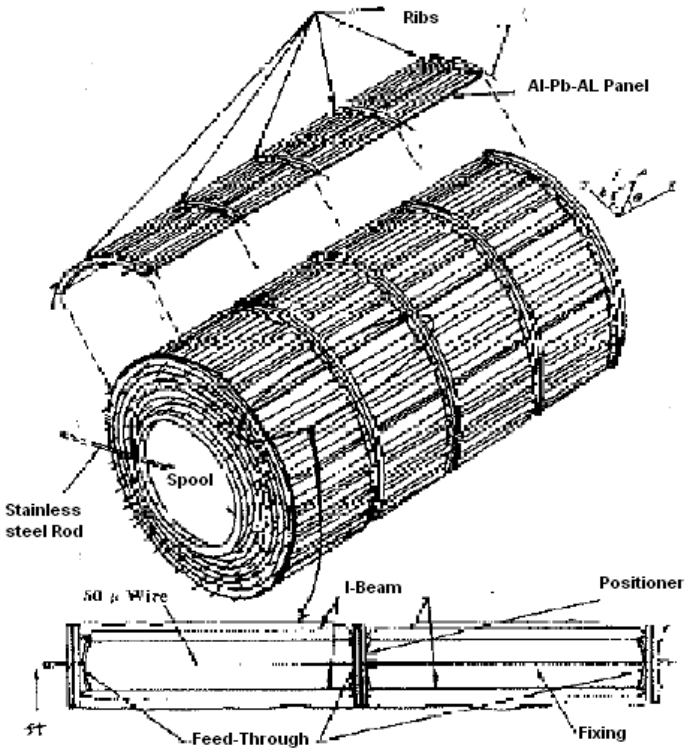

Figure 3.7: Schematic view of the barrel shower counter ([31], [35])

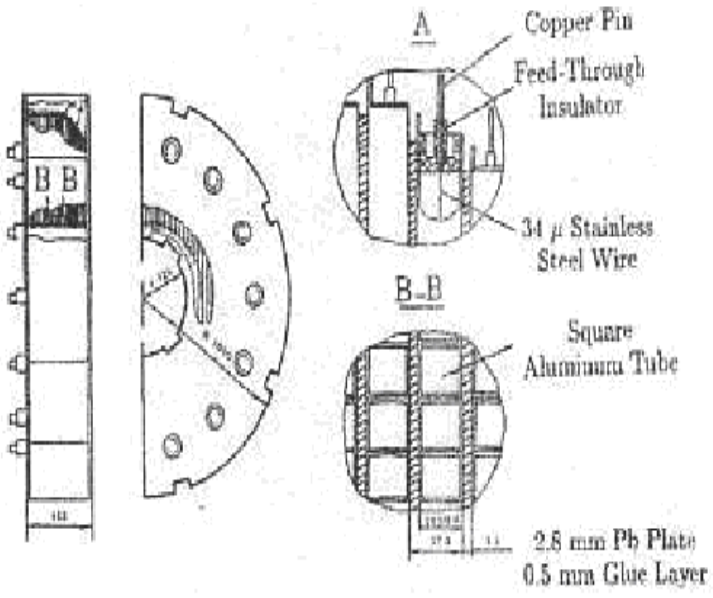

Figure 3.8: Endcap shower counter ([31], [36])

The performance of the shower counter was tested by using Bhabha events. Shower position resolution was estimated to be $\sigma_\phi = 7.9$ mm and $\sigma_z = 36$ mm for BSC while $\sigma_x = 15$ mm and $\sigma_y = 17$ mm for ESC. The energy resolution was $\triangle E/E = 21.0\%/\sqrt{E}$ and $\triangle E/E = 22.1\%/\sqrt{E}$ (E in GeV), respectively [31].

3.2.5 Muon Counter

The outermost sub-detector [37] was a 3-layer muon counter interleaved with the iron flux return outside the magnet coil. Its purpose was to identify muons with momentum greater than 0.5 GeV/c. Their proportional tubes were used to measure the track position in terms of azimuthal angle ϕ, and z-coordinate was determined through charge-division [31].

3.2.6 Luminosity measurements

The luminosity monitor [38] was mounted on both sides of the intersection region, close to the beam line. The Luminosity was determined by measuring Bhabha scattering rate at small angle with the detector. The measured value was compared with the theoretical value obtained through perturbative QED, giving an uncertainty of 3%. The luminosity monitor system is shown in Fig. 3.9. It has four group of counters, each consisting of two scintillation counters and one calorimeter. One of the scintillation counters is a defining counter P and the other one is an auxiliary counter C. The calorimeter is used to measure the shower electromagnetic energy [31].

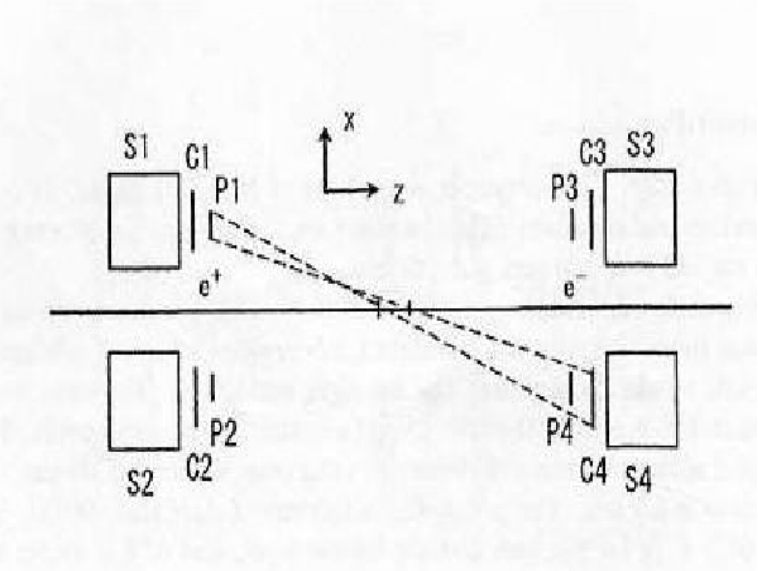

Figure 3.9: Luminosity Monitor System ([31], [38])

3.3 Software and Physics Analysis Tools

The software used for generating Monte Carlo (MC) simulation is called GENSIM and it was developed by BES group. GENSIM consists of two main drivers; GENBES and SIMBES ([39], [40]), where GENBES is the event generator and SIMBES performs the BESII detector simulation. GENBES is used within SIMBES to provide kinematic information for primary events. For simulating various J/ψ and $\psi(2S)$ radiative decays, the original MC generators were developed at MARK-III experiment. BESII detector simulation was based on GEANT3 [41] for simulating various physical processes. GENSIM produces a raw data file. This data file is used to reconstruct important physical information about the events [31].

3.4 Detector background

Detector background such as noisy electronics channels or signal distortion from unwanted interactions between the detector and the decay particles, varies from experiment to experiment. In BESII, unwanted particle interaction with the detector such as pair-production, small-angle scattering, energy-losses and bremsstrahlung, and electronics deficiencies such as noisy and dead channels are taken into account in the Monte Carlo simulation [42].

Chapter 4

Charmonium Study - A Literature Survey

As described earlier, there are six quark flavors: up, down, strange, charm, bottom and top ([3], [5]). This list has come out in decades of theoretical and experimental investigations [43]. Before November 1974, the list consisted of only three quark flavors: up, down and strange (light quark flavors). By that time charm quark had been predicted theoretically [44]. A quest for this quark was therefore going on in high energy physics laboratories. On 11th November, 1974, known as November revolution in the history of particle physics, two high energy physics laboratories (Stanford Linear Accelerator Centre (SLAC) [45] and Brookhaven National Laboratory (BNL) [46]) announced the discovery of a new resonance with *central mass* value of 3.097 GeV/c^2. It was concluded that this resonance is a composite state of a charm-anticharm pair also known as *charmonium*. This resonance is now known as J/ψ, with $j^{PC} = 1^{--}$, because it was given different names: J by BNL and ψ by SLAC. It had a very narrow width with comparatively longer lifetime of 7.2×10^{-21} sec.

The J/ψ resonance was observed in the following reactions:

At SLAC

$$e^+e^- \rightarrow \psi \rightarrow hadrons$$

At BNL

$$p + Be \rightarrow J/\psi + anything$$

with

$$J/\psi \rightarrow e^+e^-$$

Observation of J/ψ thus provided a first experimental evidence of the fourth quark i.e., charm. Second experimental confirmation of charm quark came after 10 days when a second charmonium state $\psi(2S)$ was discovered at SLAC [3]. Later on, more charmonium states ($\psi(3S)$, $\psi(4S)$, ...) were observed experimentally, further confirming the existence of charm quark. J/ψ is the ground state of its family whereas $\psi(2S)$ is its first excited state [44].

The charmonium states can decay via electromagnetic or hadronic processes involving radiative transitions or annihilation decays. The radiative transitions have mainly two types: electromagnetic and hadronic. Electromagnetic transitions involve the decay of charmonium states to their low lying charmonium states by emitting photons. In hadronic transitions, the charmonium states are converted into lower states via emission of lighter mesons such as π and ρ. The annihilation decays are of mainly

two types: hadronic and electromagnetic. In hadronic annihilation of charmonium states such as $\psi(2S)$, hadrons are predominantly formed from three gluons (Fig. 4.1). The hadronic decay modes of $\psi(2S)$ are strongly suppressed. This suppression is in accordance with OZI rule ([47], [48], [49]), justifying long lifetime of this resonance. Due to this strong suppression, the probability of electromagnetic decays of $\psi(2S)$ become comparable with that of the hadronic decays. That is why, its leptonic decays have significant branching fraction. In electromagnetic annihilation the hadrons are formed from the photons produced due to the annihilation of charm-anticharm pair (Fig. 4.1) ([42], [44]). The annihilation decays are mainly divided into two or three body intermediate state decay processes. Two body decays involve a meson pair or a baryon antibaryon pair. Three body decays may involve three mesons or a baryon antibaryon pair accompanied by a meson ([50], [51]). These decay modes provide excellent opportunities to search for hybrids, study properties of light hadrons, investigate excited hadronic states, measure mixing angles of SU(3) and probe the possibility of decay processes violating conservation laws such as lepton flavour violation, isospin violation, strangeness violation and CP violation ([7], [45], [46], [52], [53], [54]).

Many $\psi(2S)$ decay processes have been studied recently by BESII [28] and CLEO-c [55], and by old experiments such as BONANZA, MARKI, DASP, MARKII, DM2 and MARKIII ([56], [57], [58], [59], [60], [61], [62], [63]). The studied decay modes include both the two body and three body intermediate state processes. Some analyses

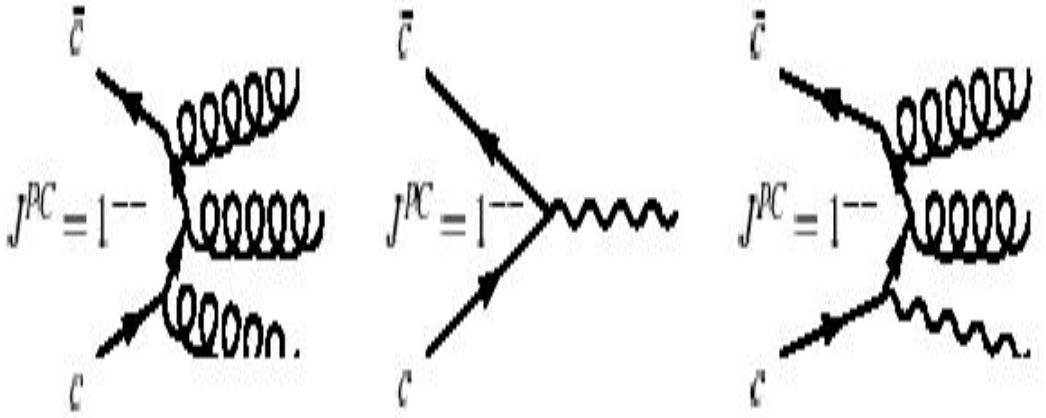

Figure 4.1: Charmonium decays through three gluons, through one photon and through one photon and two gluons [42]

deal with finding the probability of decay processes which violate certain conservation laws ([7] [64] [65] [66]).

The violation processes can also be studied using three body intermediate state processes such as isospin violating process $(J/\psi,\ \psi(2S)) \to \Lambda\bar{\Lambda}\pi^0$ studied at BESII [7]. Theoretically, formation of three hadrons in the intermediate state can be explained within the 'diquark model' [67]. According to this model, three body intermediate state may arise from the combination of quark (anti-quark) and diquark (anti-diquark) pairs formed from three gluons produced in $c\bar{c}$ pair annihilation. Fig. 4.2 shows a Feynman diagram representing the hadronization of three gluons into a three body intermediate state containing a baryon antibaryon pair and a meson [67]. The formation of such intermediate state may involve scalar diquark, vector diquark or both [67], such as $\psi(2S) \to \Lambda\bar{\Lambda}\pi^0$ decay process involves only scalar diquark.

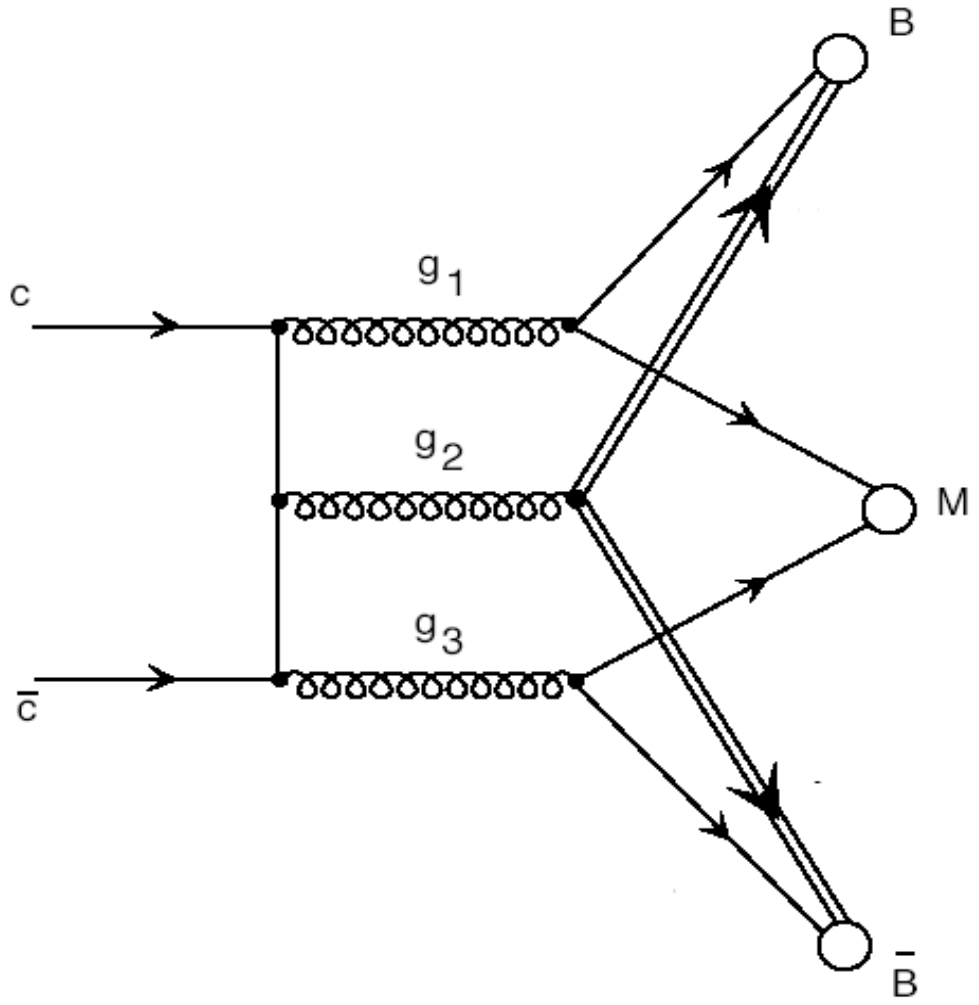

Figure 4.2: Feynman diagram representing 'diquark model', for the formation of a baryon antibaryon pair and a meson, from three gluons [67]

Our study is aimed to probe the isospin and strangeness violating decay process $\psi(2S) \rightarrow \Lambda\bar{\Lambda}K_s^0$. The intermediate state of this decay process involves a baryon antibaryon pair ($\Lambda\bar{\Lambda}$) and a pseudoscalar meson (K_s^0). The three hadrons in the

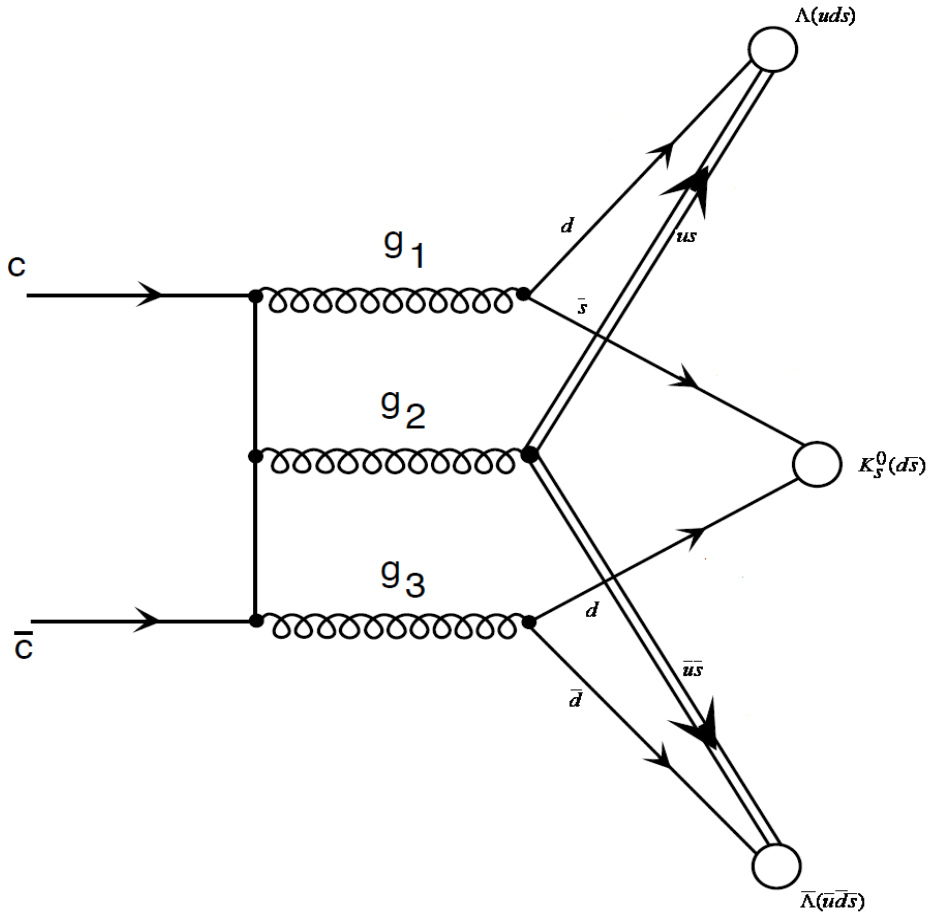

Figure 4.3: Feynman diagram representing 'diquark model', for the formation of a $\Lambda\bar{\Lambda}$ pair and a K_s^0 meson, from three gluons [67]

intermediate state can be formed only through violation of strangeness and isospin. According to 'diquark model', Fig. 4.3 shows a possible Feynman diagram for the formation of $\Lambda\bar{\Lambda}$ pair and pseudoscalar meson K_s^0. The intermediate state shown in

this figure arises through violation of strangeness and isospin at gluonic vertex g_1. We have probed the possibility of this strangeness and isospin violating process by using 14 million $\psi(2S)$ data recorded by BESII experiment. The details of our study follow in the next chapter.

Chapter 5

Analysis of $\psi(2S) \to \Lambda\bar{\Lambda}K_s^0$

5.1 Introduction

[1]The $\psi(2S)$ state is a non-relativistic bound state of $c\bar{c}$ pair. According to QCD predictions, $\psi(2S)$ decays predominantly via $c\bar{c}$ annihilation into three gluons or a virtual photon [42]. These gluons or photon lead to hadronic states obeying or violating conservation of important quantum numbers such as baryon number (b), strangeness (s), isospin (I), etc. On the non-conservation side, isospin non-conserving decay mode $J/\psi \to \Lambda\bar{\Lambda}\pi^0$ has been studied at BESI, BESII and DM2 ([7], [8], [6]) and $\psi(2S) \to \Lambda\bar{\Lambda}\pi^0$ at BESII [7]. To the best of our knowledge, no study exists in literature about the strangeness violating decays of any charmonium state such as J/ψ or $\psi(2S)$. The analysis of $\psi(2S) \to \Lambda\bar{\Lambda}K_s^0$ is therefore of prime importance as it would be the first study in this direction. The *isospin violating* process $\psi(2S) \to \Lambda\bar{\Lambda}\pi^0$ has been reported with an upper limit at 90% confidence level [7]. In our study, the case is different, because $\psi(2S) \to \Lambda\bar{\Lambda}K_s^0$ *violates the conservation of isospin as well*

[1]Results reported in this chapter are based upon BESII analysis memo entitled *Search for* $\psi(2S) \to \Lambda\bar{\Lambda}K_s^0$.

as strangeness. Keeping in view that the decay mode of $\psi(2S)$ which violates only isospin conservation is found with an upper limit, we decided to investigate some decay mode which violates isospin as well as strangeness. The objective in making such study was to probe the probability of such decay mode. Such type of studies will help to authenticate the credibility of standard model or to look for any hint beyond the standard model. The analysis of the current decay process was carried out by using about 14 million $\psi(2S)$ events registered by BESII. Details of this analysis are described in the following sections.

5.2 Monte Carlo Simulations

As indicated in section 3.3, the Monte Carlo samples of signal decay process $\psi(2S) \rightarrow \Lambda\bar{\Lambda}K_s^0$ and exclusive background channels were obtained by using 'GENSIM' program. This program is divided into two parts: 'GENBES' and 'SIMBES'([39], [40]). These programs control the process of MC event generation and detector simulation of the generated events, respectively. In order to run these programs in a sequence, 'gensim' card was used. This card has two parts: 'genbes' and 'simbes'. The 'genbes' card is used to specify MC generator name and the prerequisites for this generator. The 'simbes' card provides important options regarding BESII detector([39], [40]). Physics of simulated events is then reconstructed by performing the following steps:

- The 'gensim' command is used to generate a file of raw simulated data.
- The simulated data is then reconstructed to get an 'ndst' file by using a 'DRUNK'

(Display and ReconstrUctioN Kit) card, through 'drunk' command. The 'ndst' file thus reconstructed contains important information about the particles of reconstructed events, such as decay vertices of resonances, polar angle, energy loss, momentum, etc.

- The reconstructed events contain information that can be used to select events satisfying specific criteria. The events which do not satisfy the selection criteria are skipped.

In the following section, we outline the criteria for initial selection of events from 'ndst' file.

5.3 Initial Event selection

Charged particles of the candidate events for the signal process: $\psi(2S) \rightarrow \Lambda\bar{\Lambda}K_s^0$, were required to satisfy the following conditions [68]:

- Each charged track is reconstructed from MDC with good helix fit (Mfit=2)
- Each charged track satisfies the vertex constraints: $R_{xy} < 12$cm , $|Rz| < 30$cm
- Transverse momentum of each charged track is such that $P_{xy} > 50$ MeV/c
- Polar angle for each track in MDC satisfies $|cos\theta| < 0.8$
- The total number of charged tracks satisfying above conditions should be six with net charge 0.

5.4 Particle Identification

After initial selection of events, it is required to reconstruct the signals of Λ, $\bar{\Lambda}$ and K_s^0 from the information of each selected event. For this purpose, each track of an event, was assigned a particle hypothesis through the process of particle identification. The process of particle identification was based on two types of information: energy loss (dE/dx) and TOF. Their theoretical and measured values were used to obtain $\chi^2_{dE/dx}$ and χ^2_{TOF}. First, the measured values of dE/dx and TOF were corrected, then the corrected measured values and the theoretical ones were used in the following relations:

$$\chi_{TOF}(i) = \frac{TOF_{meas} - TOF_{exp}(i)}{\sigma_{TOF}(i)}$$

$$\chi_{dE/dx}(i) = \frac{dE/dx_{meas} - dE/dx_{exp}(i)}{\sigma_{dE/dx}(i)},$$

where TOF_{meas}, $TOF_{exp}(i)$, $\sigma_{TOF}(i)$, dE/dx_{meas}, $dE/dx_{exp}(i)$ and $\sigma_{dE/dx}(i)$ represent the corrected measured values, expected values and resolutions of TOF and dE/dx, respectively, used for a particle hypothesis i.

Using the above relations, the $\chi^2_{dE/dx}(i)$ and $\chi^2_{TOF}(i)$ values were obtained for a particle hypothesis i assumed for each track in the event. For a positively or a negatively charged particle, three pairs of values for $\chi^2_{dE/dx}(i)$ and $\chi^2_{TOF}(i)$, were evaluated. A combined χ^2 value was calculated for each hypothesis i, by adding the individual values for that hypothesis:

$$\chi^2(i) = \chi^2_{TOF}(i) + \chi^2_{dE/dx}(i),$$

where i represents proton(p) or positive pion (π^+) or positive kaon (K^+) for a positive particle hypothesis and anti-proton ($\bar{p}$) or negative pion π^- or negative kaon (K^-) for a negative particle hypothesis. Once the combined χ^2 values were ready for each particle hypothesis, each track (particle) of an event was identified as a particular hypothesis by using the following comparisons:

- Positive pion (π^+) was identified if the following inequality was satisfied:

$$\chi^2(\pi^+) < \chi^2(K^+) \text{ and } \chi^2(\pi^+) < \chi^2(p).$$

- Proton identification was performed through the following inequality:

$$\chi^2(p) < \chi^2(K^+) \text{ and } \chi^2(p) < \chi^2(\pi^+).$$

- Negative pion (π^-) was identified by using the following inequality:

$$\chi^2(\pi^-) < \chi^2(K^-) \text{ and } \chi^2(\pi^-) < \chi^2(\bar{p}).$$

- Anti-proton ($\bar{p}$) was identified through the following comparison:

$$\chi^2(\bar{p}) < \chi^2(K^-) \text{ and } \chi^2(\bar{p}) < \chi^2(\pi^-).$$

Success of particle identification process was based on the criteria that there should be two positive pion, two negative pion, a proton and an anti-proton, meaning all particles are identified.

5.5 Secondary Vertex Fit

After successful particle identification, the pion belonging to Λ, $\bar{\Lambda}$ and K_s^0 were determined through secondary vertex fitting. As we know that there are two positive pion

and two negative pion in the final state of $\psi(2S) \to \Lambda\bar{\Lambda}K_s^0$, we applied vertex fitting to the possible $p\pi^-$, $\bar{p}\pi^+$ and $\pi^+\pi^-$ combinations, by using 'KLAMS' vertex fitting algorithm, for searching decay products of Λ, $\bar{\Lambda}$ and K_s^0. The combinations passing vertex fitting and with minimal value of $|M_{p\pi^-} - M_\Lambda| + |M_{\bar{p}\pi^+} - M_{\bar{\Lambda}}| + |M_{\pi^+\pi^-} - M_{K_s^0}|$, were accepted for kinematic fitting.

5.6 Kinematic Fit

After getting $p\pi^-$, $\bar{p}\pi^+$ and $\pi^+\pi^-$ combinations successfully from vertex fitting, we applied four-constraint (4C) kinematic fit to the hypothesis $\psi(2S) \to p\,\bar{p}\,2(\pi^+)\,2(\pi^-)$, imposing conservation of total energy and momentum and $\chi^2_{4C} < 50$. All the MC and data events were passed through 4C kinematic fit. The events passing 4C fit successfully were used to reconstruct the invariant mass distributions $p\pi^-$, $\bar{p}\pi^+$ and $\pi^+\pi^-$ to represent the Λ, $\bar{\Lambda}$ and K_s^0. Samples of these invariant mass spectra, alongwith χ^2_{4C}, the Λ, $\bar{\Lambda}$ and K_s^0 decay lengths, etc, were saved into 'HBOOK' files. A comparison of χ^2_{4C} distributions of MC and data events is shown in Fig. 5.1.

5.7 Determination of Mass Resolutions

After 4C kinematic fit, the invariant mass spectra of $p\pi^-$, $\bar{p}\pi^+$ and $\pi^+\pi^-$ were fit with single gaussian function. From the fit results as shown in Fig. 5.2 and Fig. 5.3, mass resolutions of Λ, $\bar{\Lambda}$ and K_s^0, were determined to be 0.0024 GeV/c^2, 0.0024 GeV/c^2 and 0.0078 GeV/c^2, respectively [68].

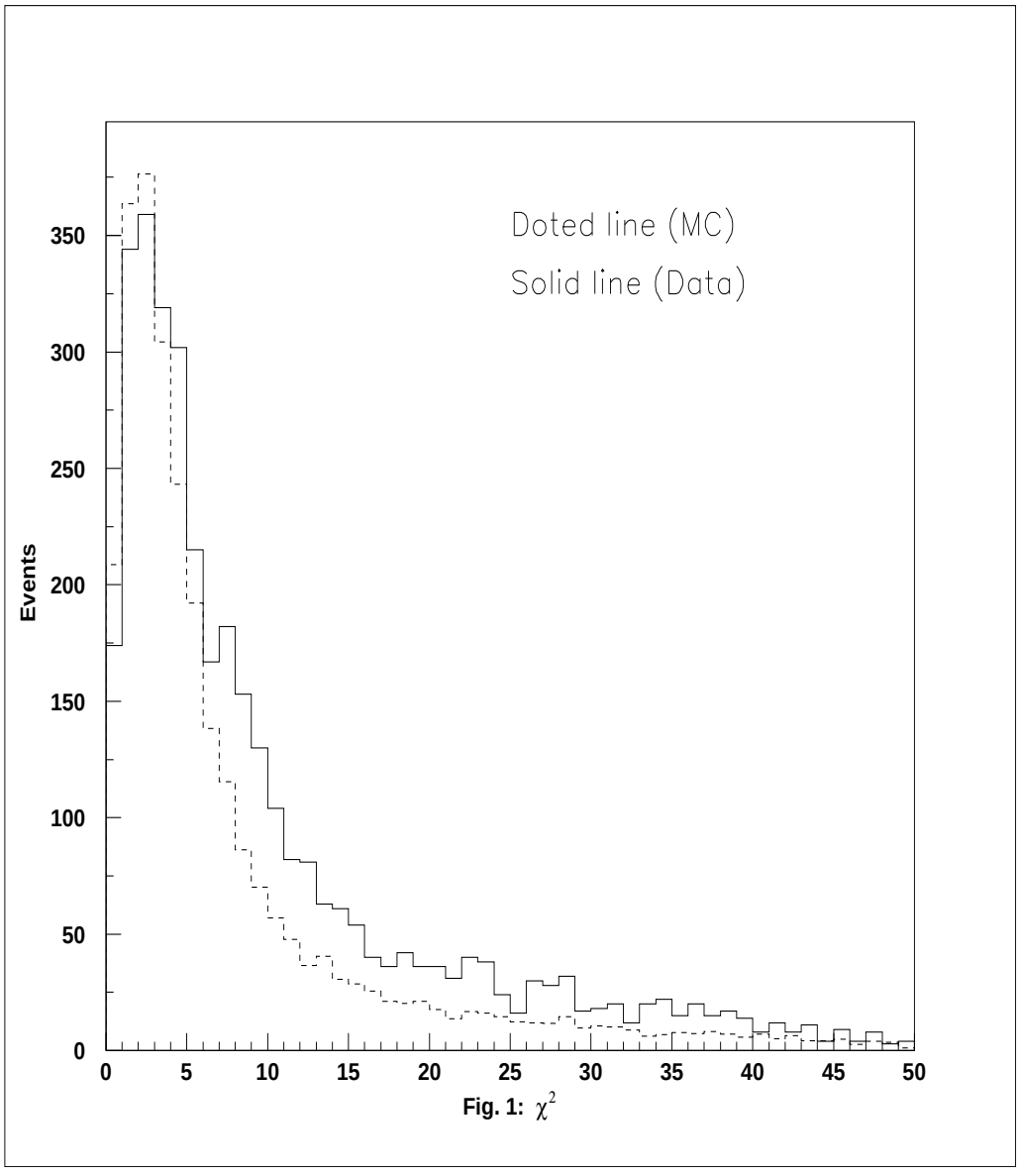

Figure 5.1: Comparison of χ^2_{4C} distributions: the dotted histogram is for MC and the solid one represents data [68].

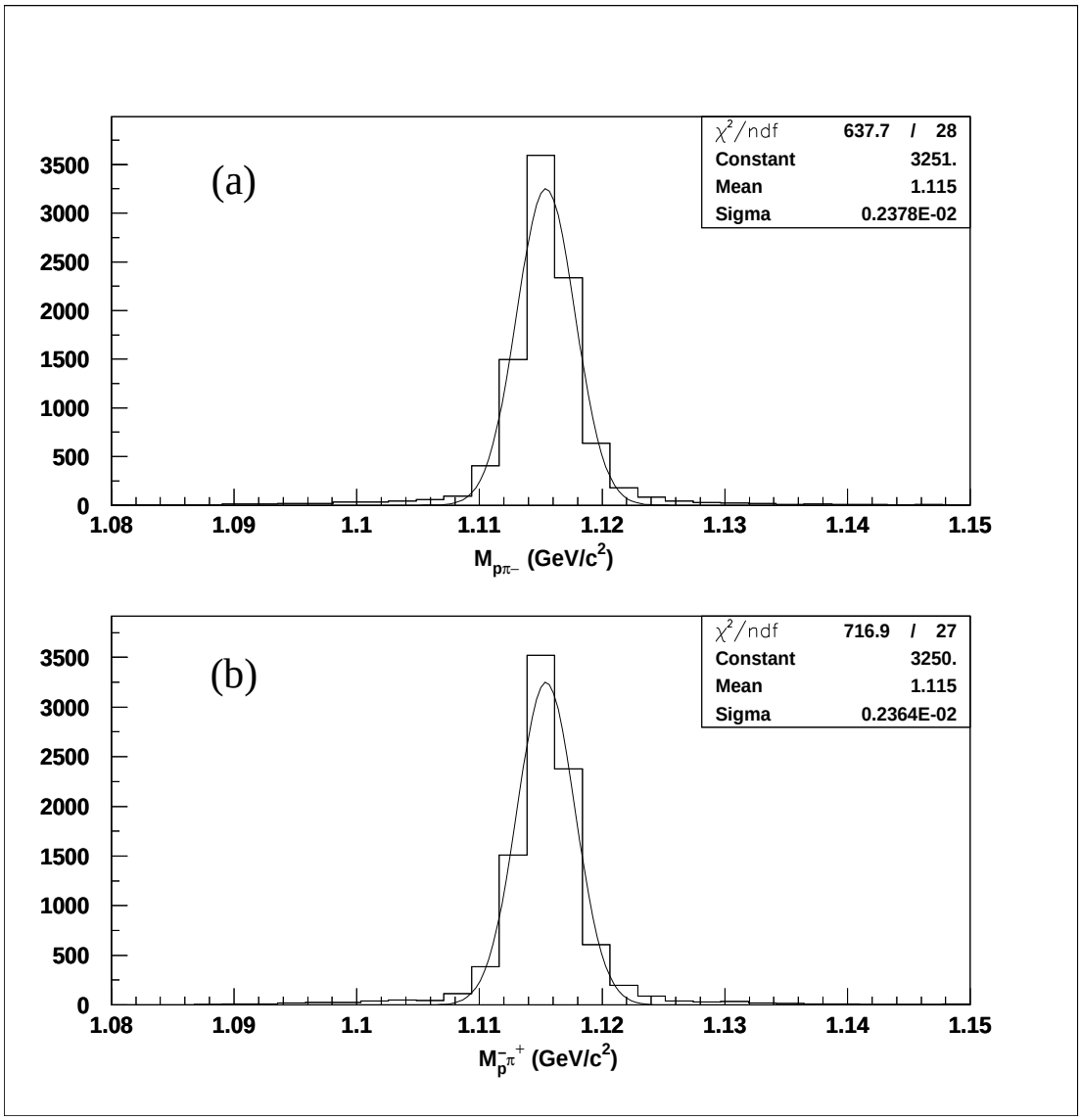

Figure 5.2: Gaussian fit for invariant mass of $p\pi^-$ and $\bar{p}\pi^-$ [68]

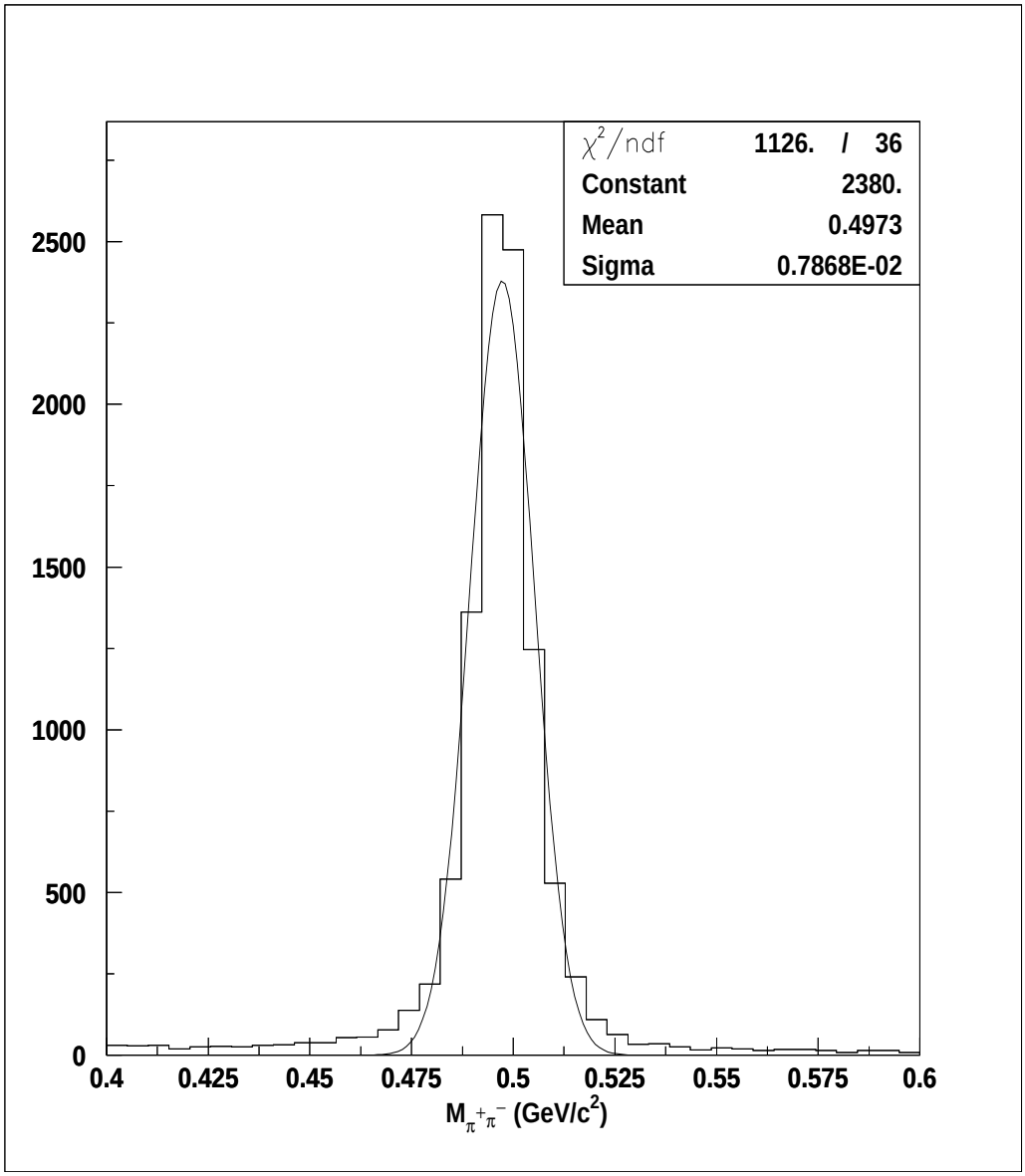

Figure 5.3: Gaussian fit for invariant mass of $\pi^+\pi^-$ [68]

5.8 Final Selection Criteria

For making final selection of events, the Λ, $\bar{\Lambda}$ and K_s^0 mass constraints were decided by using their mass resolutions. Their invariant mass spectra were constrained to be within 3σ from the corresponding central mass values, where σ represents the mass resolution. In this way the following mass constraints were decided:

- $|M_{p\pi^-} - M_{\Lambda}| < 0.008$ GeV/c^2
- $|M_{\bar{p}\pi^+} - M_{\bar{\Lambda}}| < 0.008$ GeV/c^2
- $|M_{\pi^+\pi^-} - M_{K_s^0}| < 0.02$ GeV/c^2,

  where $M_{\Lambda,\bar{\Lambda}} = 1.1156$ GeV/c^2 and $M_{K_s^0} = 0.4976$ GeV/c^2.

In addition to mass constraints, the cuts for secondary vertices of Λ, $\bar{\Lambda}$ and K_s^0 were also decided as a part of final selection criteria. To reject the backgrounds from the channels which don't include Λ but K_s^0 , we required the vertex constraint $R_{xy} > 5$mm (where R_{xy} is the distance from reconstructed vertex of $\Lambda(\bar{\Lambda})$ to the original point of $\Lambda(\bar{\Lambda})$).

Similarly, to reject the background from channels which don't include K_s^0, we required $R_{xy} > 5$mm [69]. One more constraint was included in the final selection criteria i.e. $\chi^2_{4C} < 25$. This constraint was decided, through optimization of χ^2_{4C}, by applying all mass and secondary vertex constraints (as described above). The χ^2_{4C} value that maximizes $\frac{S}{\sqrt{S+B}}$, was chosen for χ^2_{4C} constraint, where S represents the MC signal and (S+B) represents signal plus background from data. The optimized χ^2_{4C} is shown

in Fig. 5.4.

5.9 Final Event Selection

The final selction of invariant mass spectra $p\pi^-$, $\bar{p}\pi^+$ and $\pi^+\pi^-$ was made under $\chi^2_{4C} < 25$ as below:

The invariant mass plot of $p\pi^-$ (Fig. 5.5 (a, b)) was selected under the following constraints:

- $|M_{\bar{p}\pi^+} - M_{\bar{\Lambda}}| < 0.008$ GeV/c^2
- $|M_{\pi^+\pi^-} - M_{K^0_s}| < 0.02$ GeV/c^2
- $|R_{xy(\Lambda)}| > 0.005$ m
- $|R_{xy(\bar{\Lambda})}| > 0.005$ m
- $|R_{xy(K^0_s)}| > 0.005$ m

The invariant mass plot $\bar{p}\pi^+$ after the following cuts is shown in Fig. 5.5 (c, d):

- $|M_{p\pi^-} - M_{\Lambda}| < 0.008$ GeV/c^2
- $|M_{\pi^+\pi^-} - M_{K^0_s}| < 0.02$ GeV/c^2
- $|R_{xy(\Lambda)}| > 0.005$ m
- $|R_{xy(\bar{\Lambda})}| > 0.005$ m
- $|R_{xy(K^0_s)}| > 0.005$ m

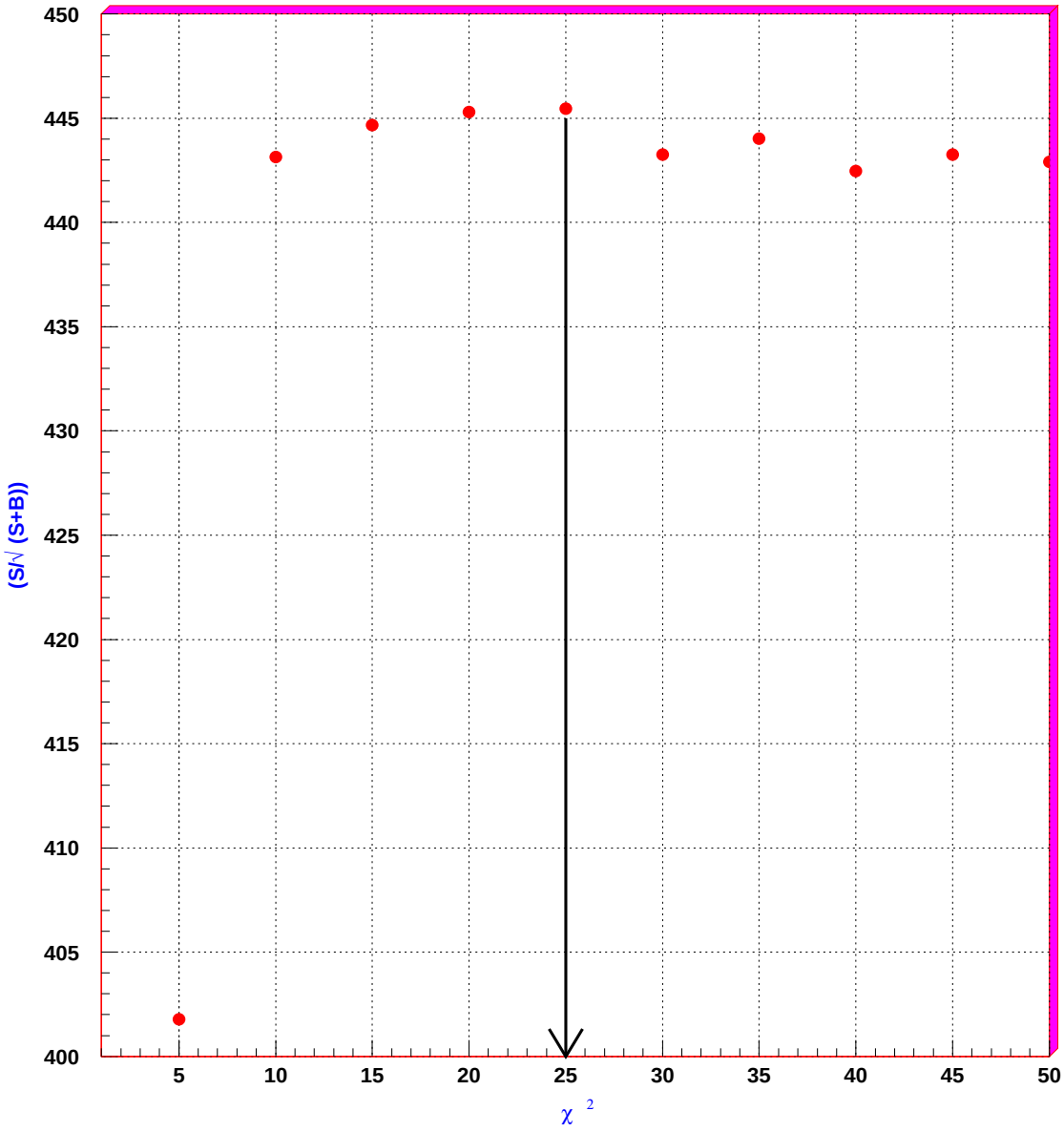

Figure 5.4: Optimized χ^2_{4C} [68]

The invariant mass plot $\pi^+\pi^-$, after the following cuts is shown in Fig. 5.5 (e, f):

- $|M_{p\pi^-} - M_{\Lambda}| < 0.008$ GeV/c^2
- $|M_{\bar{p}\pi^+} - M_{\bar{\Lambda}}| < 0.008$ GeV/c^2
- $|R_{xy(\Lambda)}| > 0.005$ m
- $|R_{xy(\bar{\Lambda})}| > 0.005$ m
- $|R_{xy(K^0_s)}| > 0.005$ m

By using the above selection criteria, clear signal of Λ and $\bar{\Lambda}$ is seen in data, as shown in Fig. 5.5. But in case of K^0_s there is no obvious signal seen in data. Comparison of data and MC are also shown in Fig. 5.5. For further investigation the scatter plots of $M_{\pi^+\bar{p}}$ versus M_{π^-p} and M_{π^-p} versus K^0_s, are shown in Fig. 5.6. One can easily find the signal of Λ and $\bar{\Lambda}$ from Fig. 5.6 (b). But, in case of K^0_s signal, it is not clear as shown in Fig. 5.6 (d). In order to know the sources of events in the signal region, background study was performed as described in the next section.

5.10 Background Analysis

5.10.1 Exclusive Background Estimation

There exist several methods for background estimation: one way is to check the similar final state of $\psi(2S)$ decays listed in Particle Data Group (PDG). The background may come from $\psi(2S) \to \Xi(1321)^-\bar{\Xi}(1321)^+$, $\psi(2S) \to \Sigma(1385)^+\bar{\Sigma}(1385)^-$ and $\psi(2S) \to$

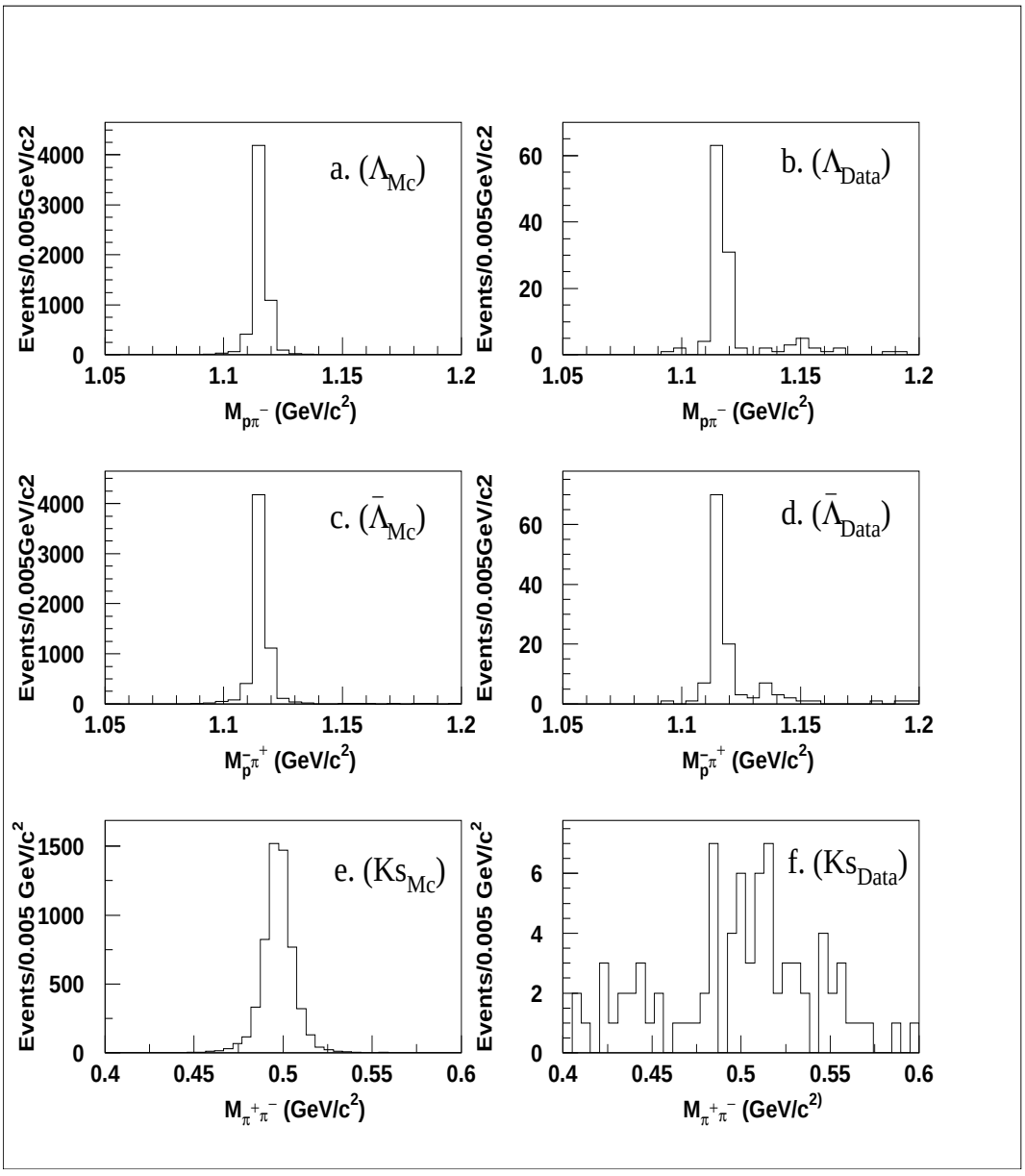

Figure 5.5: Invariant mass plots of Λ, $\bar{\Lambda}$ and K^0_s: (a) $M_{p\pi^-}$ in MC. (b) $M_{p\pi^-}$ in data (c) $M_{\bar{p}\pi^+}$ in MC. (d) $M_{\bar{p}\pi^+}$ in data (e) $M_{\pi^+\pi^-}$ in MC (f) $M_{\pi^+\pi^-}$ in data [68]

.

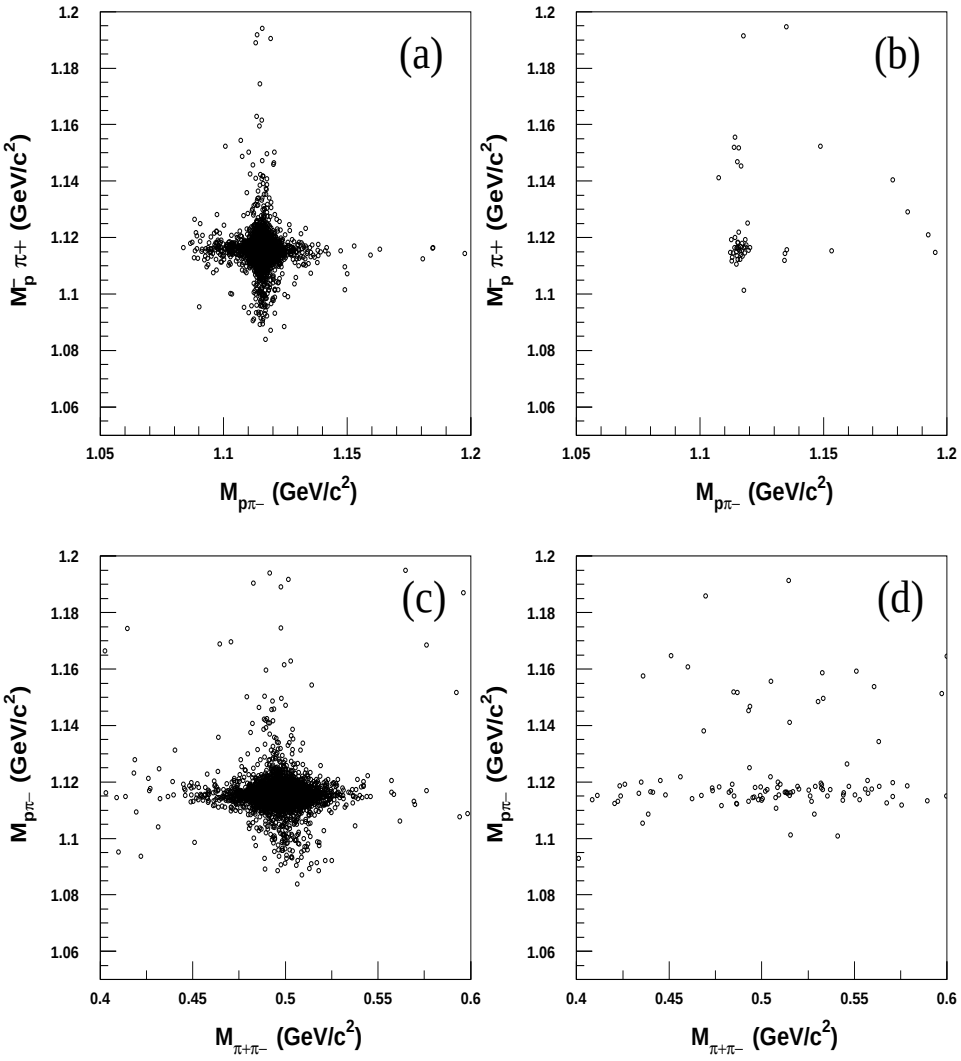

Figure 5.6: Scatter plots: (a). $M_{\pi^+\bar{p}}$ versus M_{π^-p} (MC), (b). $M_{\pi^+\bar{p}}$ versus M_{π^-p} (data), (c). $M_{\pi^+\pi^-}$ versus M_{π^-p} (MC), (d). $M_{\pi^+\pi^-}$ versus M_{π^-p} (data) [68]

$\Lambda\bar{\Lambda}\pi^+\pi^-$ channels. For these channels, the invariant mass plots of $p\pi^-\pi^-$, $p\pi^-\pi^+$ and $\Lambda\bar{\Lambda}$ from data are shown in Fig. 5.7(a), Fig. 5.7(b) and Fig. 5.8. From Fig. 5.7(a), we found the signal near 1.321 GeV/c^2 which is for $\Xi(1321)$ and same is for the $\bar{p}\pi^+\pi^+$. From these plots, it is clear that main background is coming from $\psi(2S) \to \Xi(1321)^-\bar{\Xi}(1321)^+$ and $\psi(2S) \to J/\psi\pi^+\pi^-$ process. However, prominent contribution amongst these two channels is from plot of $\Lambda\bar{\Lambda}$, which emerges from J/ψ (Fig. 5.8).

To suppress these background channels, we generated 50,000 MC events using HOWL generator and found the mass resolutions of Ξ^- and J/ψ, by fitting $p\pi^-\pi^-$ and $\Lambda\bar{\Lambda}$ invariant mass spectra, as shown in Fig. 5.9 and Fig. 5.10.

To suppress the background from two main channels $\psi(2S) \to J/\psi\pi^+\pi^-$, with $J/\psi \to \Lambda\bar{\Lambda}$ and $\psi(2S) \to \Xi(1321)^-\bar{\Xi}(1321)^+$, we used 3 σ mass cuts:

$|M_{\Lambda\pi^-} - 1.321| > 0.012$ GeV/c^2

$|M_{\bar{\Lambda}\pi^+} - 1.321| > 0.012$ GeV/c^2

$|M_{\Lambda\bar{\Lambda}} - 3.0976| > 0.02$ GeV/c^2

5.10.2 Inclusive Background estimation

Background study was also carried out using MC sample of 14 M $\psi(2S) \to$ anything, generated by Lund charm generator [70]. In this study, the K_s^0 mass window was used to look for background channels. The background channels with $|M_{\pi^+\pi^-} - 0.4976| <$ 0.02 GeV/c^2 are:

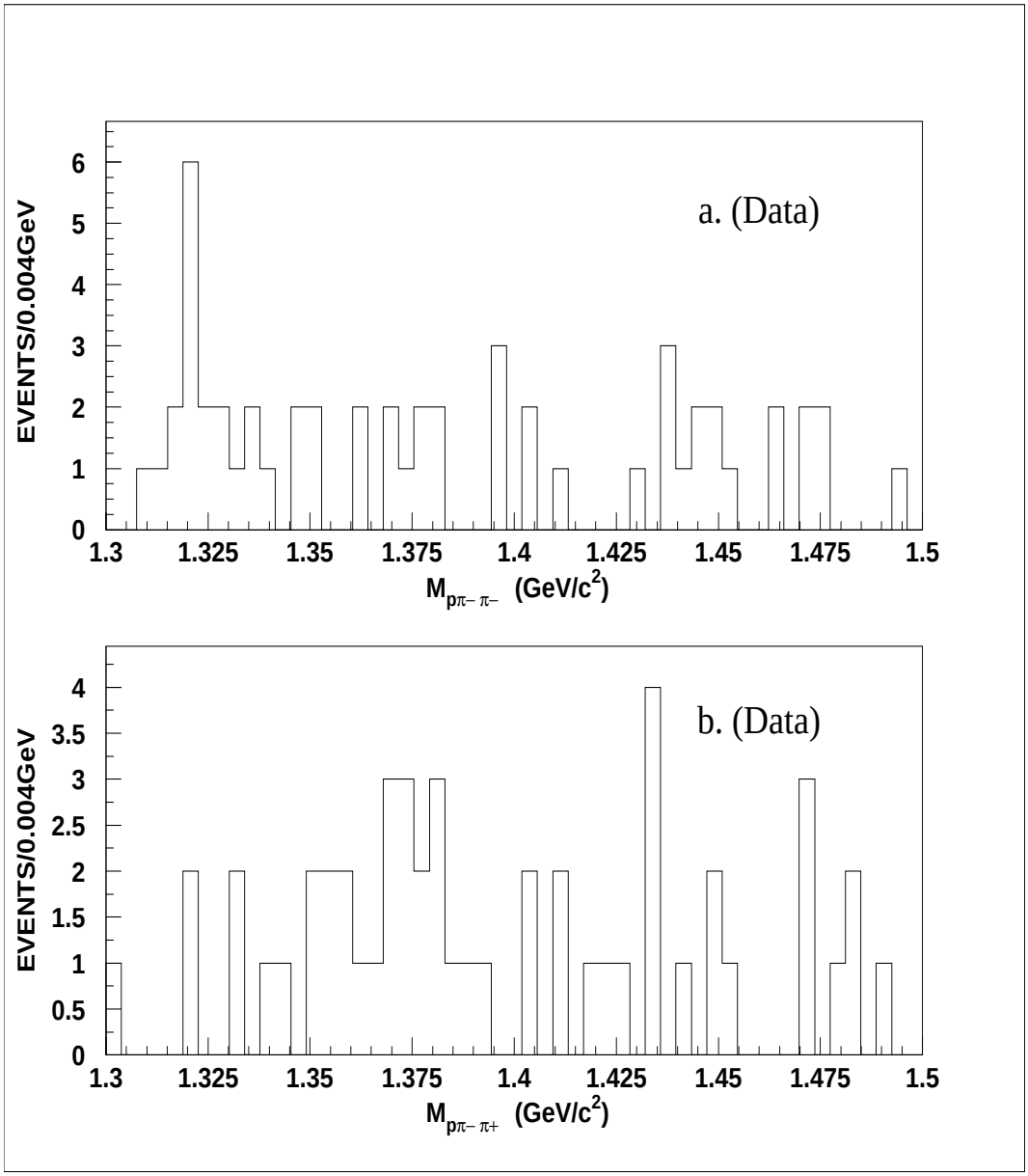

Figure 5.7: The background invariant mass distributions in $\psi(2S) \to \Lambda\bar{\Lambda}K_s^0$: (a) invariant mass of $p\pi^-\pi^-$ (b) invariant mass of $p\pi^-\pi^+$. [68]

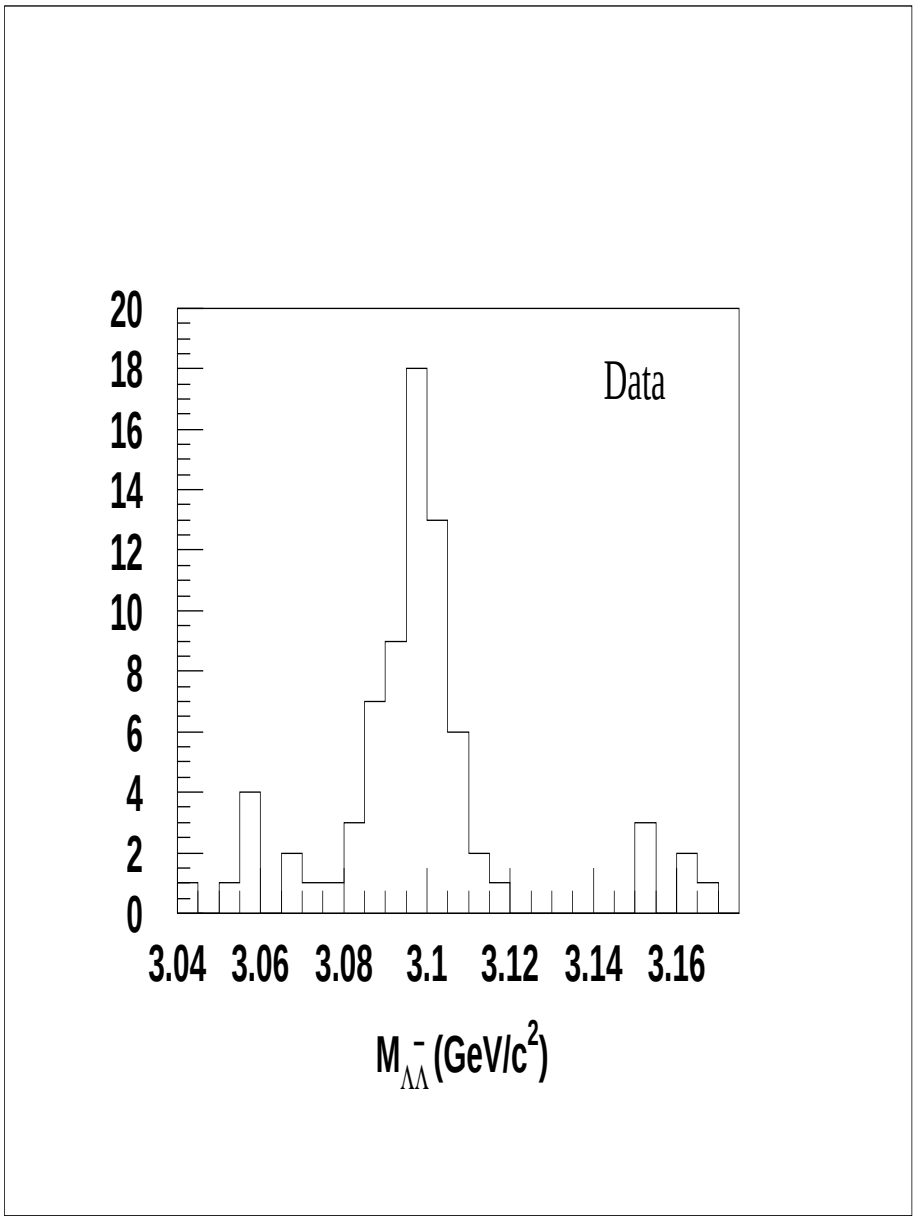

Figure 5.8: Invariant mass of $\Lambda\bar{\Lambda}$ from $\psi(2S) \to \Lambda\bar{\Lambda}K_s^0$ [68]

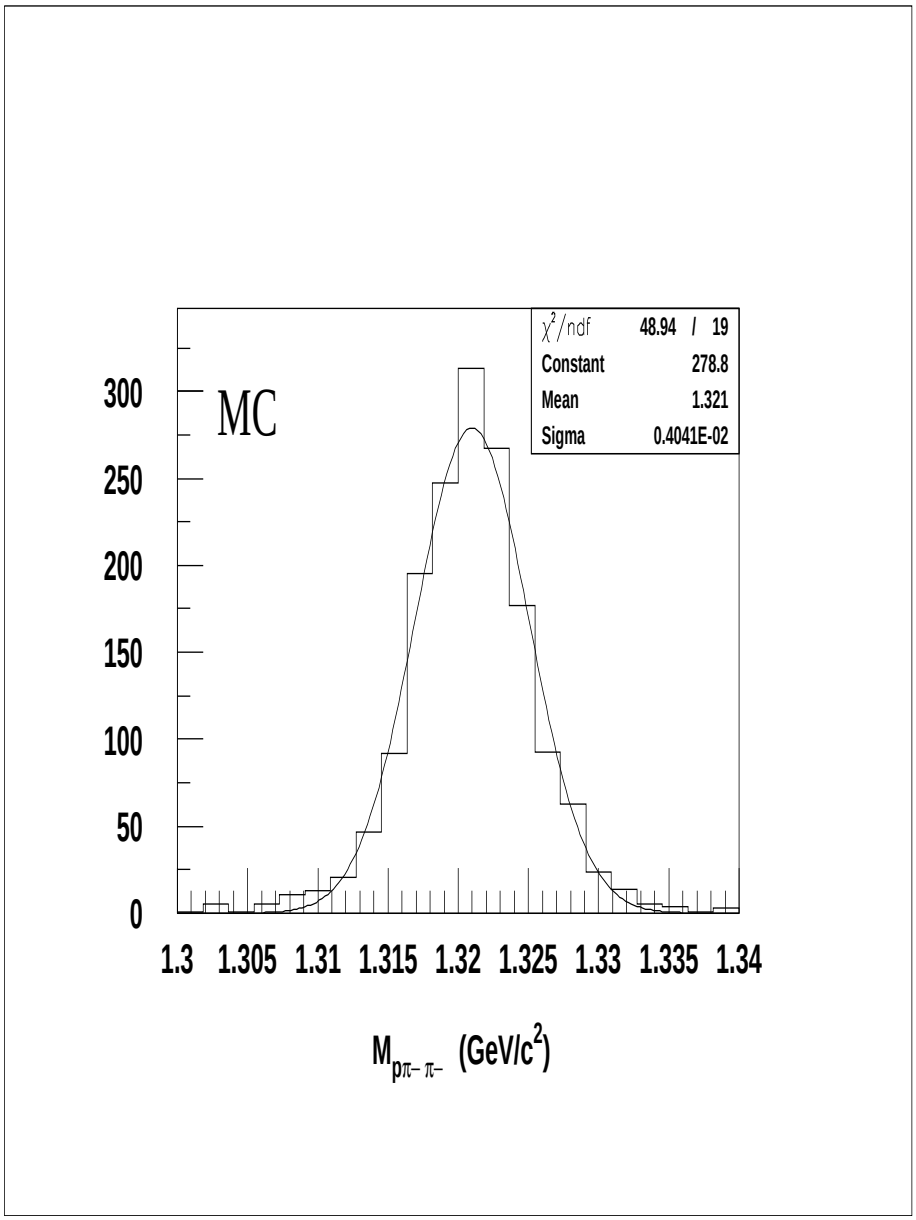

Figure 5.9: Invariant mass of $p\pi^-\pi^-$ from MC ($\psi(2S) \to \Xi(1321)^-\bar{\Xi}(1321)^+$) [68]

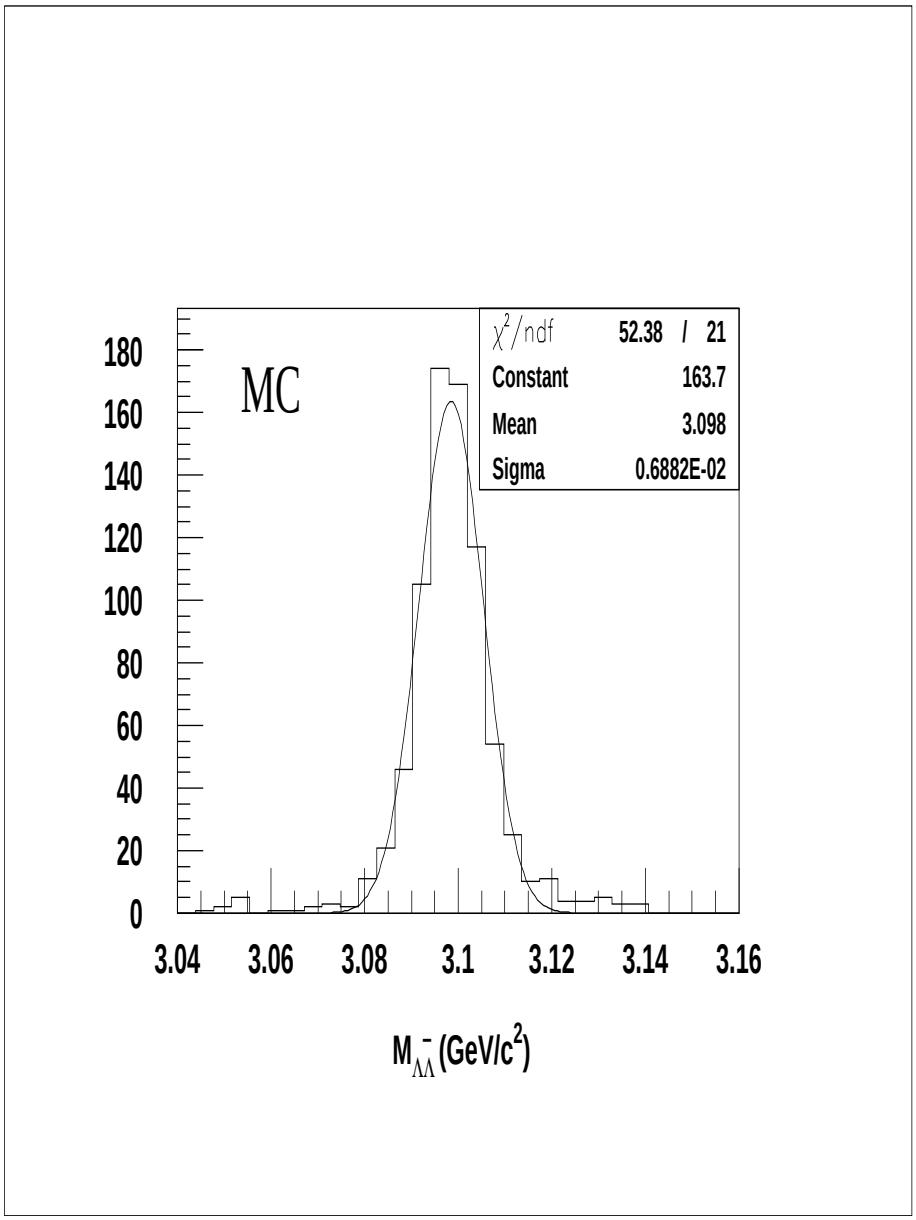

Figure 5.10: Invariant mass of $\Lambda\bar{\Lambda}$ from MC ($\psi(2S) \to J/\psi\pi^+\pi^-, J/\psi \to \Lambda\bar{\Lambda}$) [68]

1. $\psi(2S) \to \bar{\Lambda} K^{*-} p$, where $K^{*-} \to \bar{K_0}\pi^-$ and $\bar{K_0} \to K_s^0$

2. $\psi(2S) \to J/\psi\pi^+\pi^-$, where $J/\psi \to \bar{\Lambda}\Sigma^0$ and $\Sigma^0 \to \Lambda\gamma$

3. $\psi(2S) \to J/\psi\pi^+\pi^-$, where $J/\psi \to \Lambda\bar{\Lambda}$

4. $\psi(2S) \to \Sigma^{*-}\pi^+\bar{\Lambda} + c.c$, where $\Sigma^{*-} \to \Lambda\pi^-$

The contribution from these channels is very small. The number of events from first two channels is one, from third channel is four and from fourth is six. The channel two and three are suppressed by imposing the mass cut of J/ψ in the range of $|M_{\Lambda\bar{\Lambda}} - 3.0976| > 0.045$ GeV/c^2, which is taken from MC of $\psi(2S) \to J/\psi\pi^+\pi^-$, where $J/\psi \to \bar{\Lambda}\Sigma^0$ and $\Sigma^0 \to \Lambda\gamma$ as shown in Fig. 5.11. We see from Fig. 5.10 and Fig. 5.11 that there are two different mass resolutions corresponding to J/ψ invariant mass of $\Lambda\bar{\Lambda}$. Another approach is used to remove the background from J/ψ resonances by taking the recoil mass of $\pi^+\pi^-$. In this way, the 'mass resolution' of recoil $\pi^+\pi^-$ mass is found from inclusive MC, within 3σ, to be 0.02 GeV/c^2. The recoil mass plots of MC and data are shown in Fig. 5.12 and Fig. 5.13, respectively. After using the final selection criteria, the invariant mass plot $\pi^+\pi^-$ obtained from $\psi(2S) \to$ anything is shown in Fig. 5.14. Events within the mass window of K_s^0 are due to the background channels: $\psi(2S) \to \Sigma^{*-}\pi^+\bar{\Lambda} + c.c$, where $\Sigma^{*-} \to \Lambda\pi^-$, shown in Fig. 5.15.

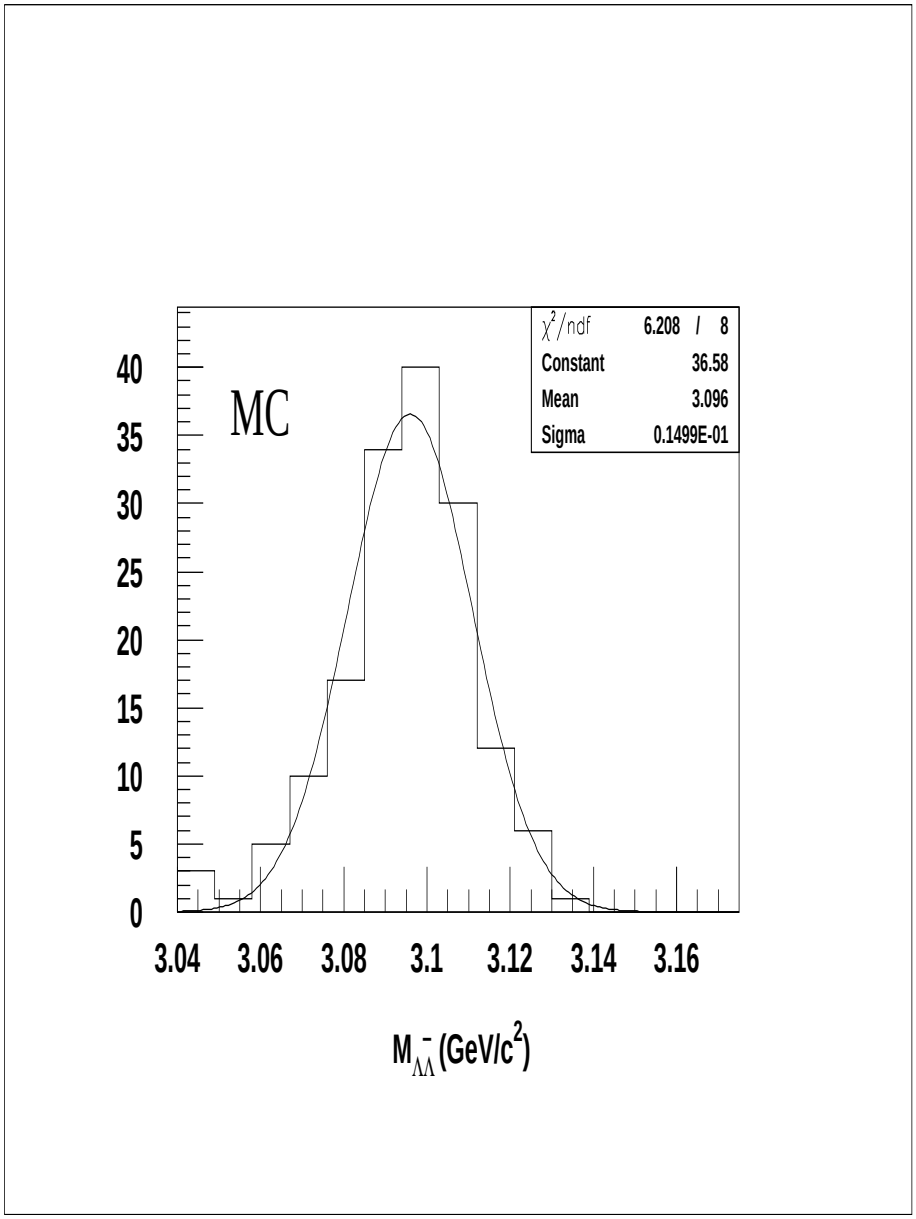

Figure 5.11: Invariant mass of $\Lambda\bar{\Lambda}$ from MC ($\psi(2S) \to J/\psi\pi^+\pi^-$, where $J/\psi \to \bar{\Lambda}\Sigma^0$ and $\Sigma^0 \to \Lambda\gamma$) [68]

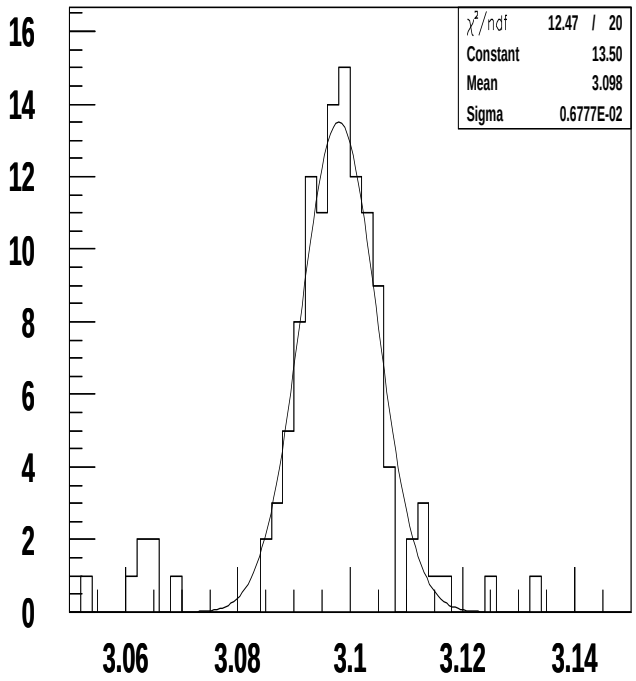

Figure 5.12: Recoil mass of $\pi^+\pi^-$ from inclusive MC for $\psi(2S) \to \Lambda\bar{\Lambda}K_s^0$ [68]

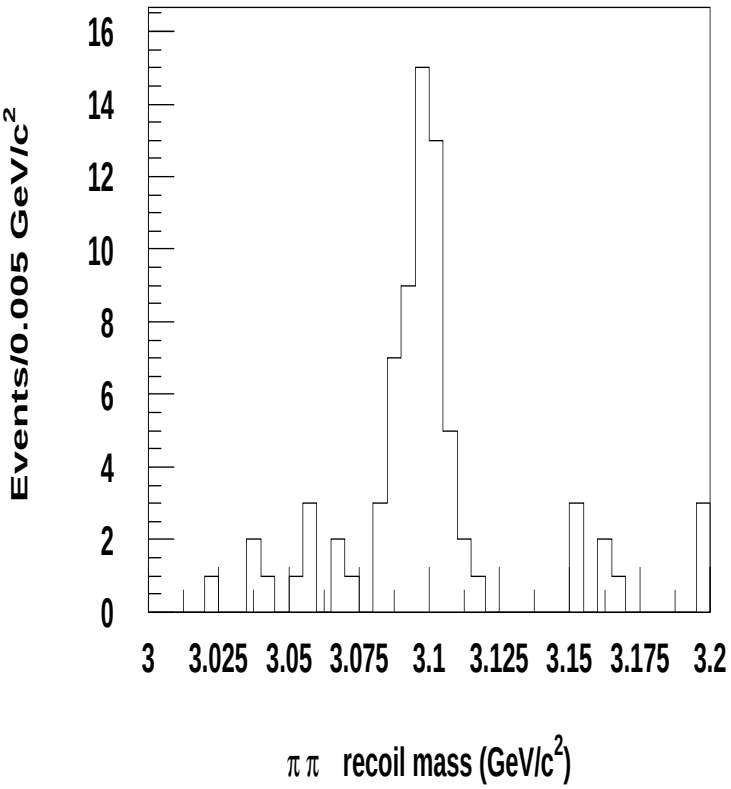

Figure 5.13: Recoil mass of $\pi^+\pi^-$ from data, for $\psi(2S) \to \Lambda\bar{\Lambda}K_s^0$ [68]

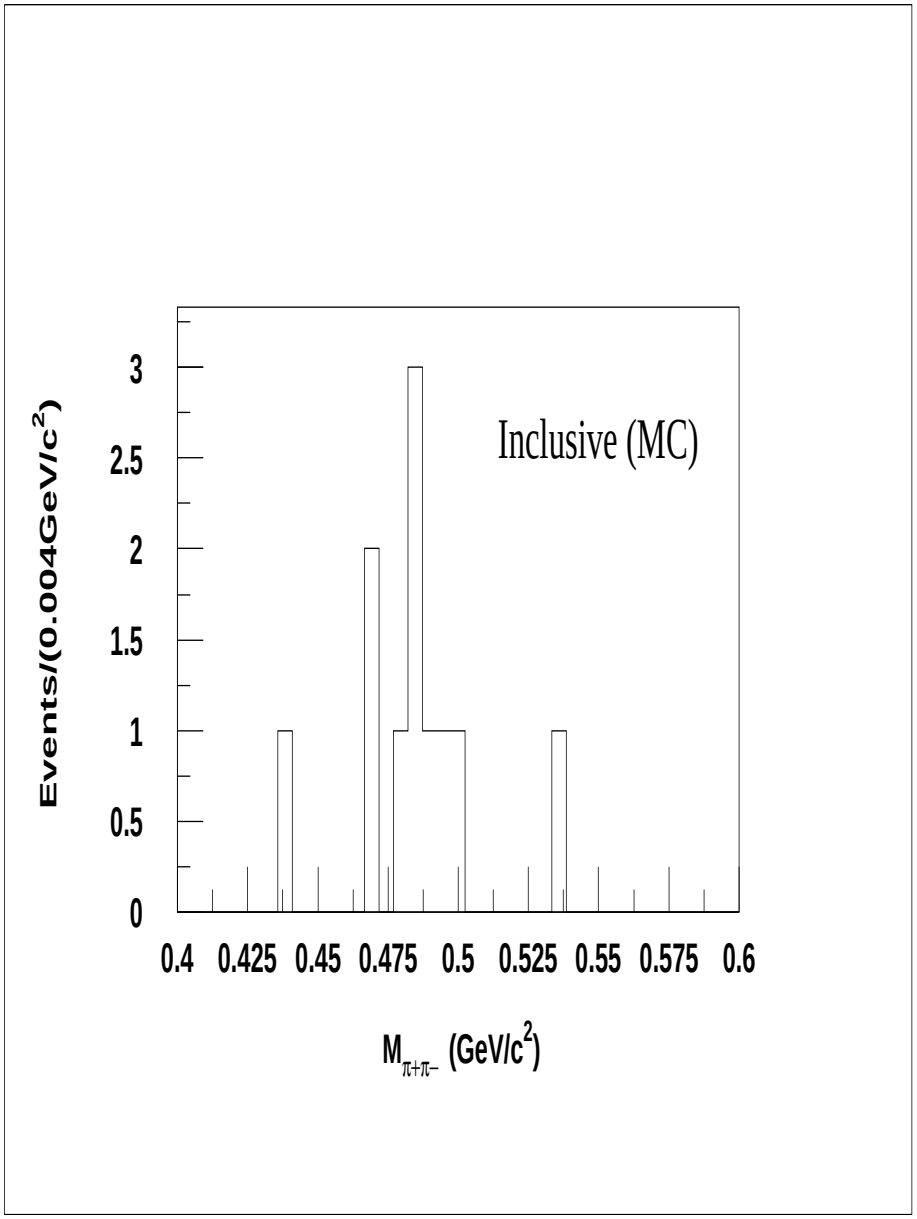

Figure 5.14: The invariant mass distribution of $\pi^+\pi^-$, from $\psi(2S) \rightarrow$ anything [68]

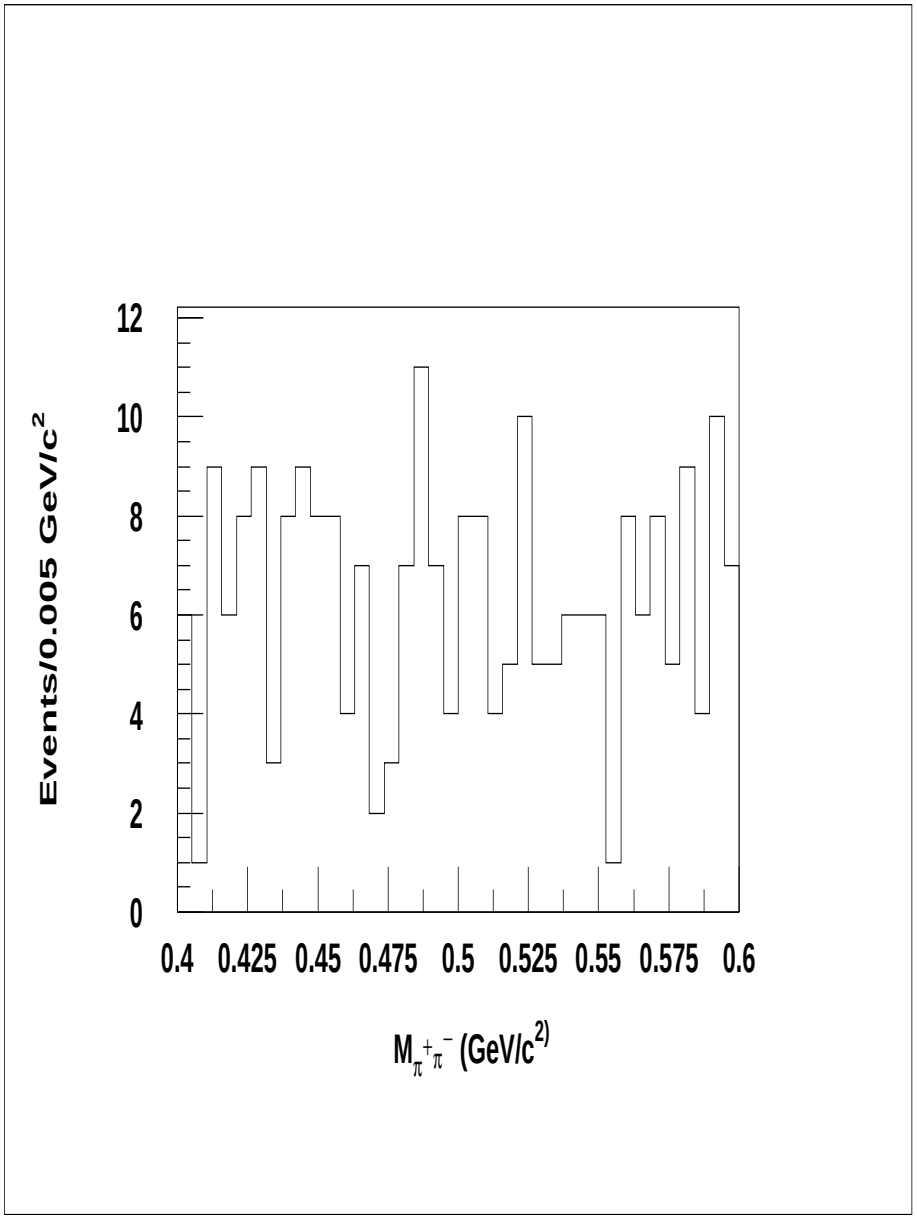

Figure 5.15: The invariant mass distribution of $\pi^+\pi^-$, obtained from $\psi(2S) \to \Sigma^{*-}\pi^+\bar{\Lambda} + c.c$, where $\Sigma^{*-} \to \Lambda\pi^-$ [68]

5.11 Final Invariant Mass Spectra After Background Subtraction

In our analysis channel $\psi(2S) \to \Lambda\bar{\Lambda}K_s^0$, the invariant mass spectra: $p\pi^-$, $\bar{p}\pi^+$ and $\pi^+\pi^-$, under final selection criteria and background elimination, are shown in Fig. 5.16. In K_s^0 mass spectrum, survived events satisfy the following selection criteria:

- $|M_{p\pi^-} - 1.1156| < 0.008$ GeV/c^2
- $|M_{\bar{p}\pi^+} - 1.1156| < 0.008$ GeV/c^2
- $|R_{xy(\Lambda)}| > 0.005$ m
- $|R_{xy(\bar{\Lambda})}| > 0.005$ m
- $|R_{xy(K_s^0)}| > 0.005$ m
- $|M_{\Lambda\pi^-} - 1.321| > 0.012$ GeV/c^2
- $|M_{\bar{\Lambda}\pi^+} - 1.321| > 0.012$ GeV/c^2
- $|RecoilMass_{\pi^+\pi^-} - 3.0976| > 0.02$ GeV/c^2

From Fig. 5.16, it is clear that no obvious signal of K_s^0 is found, so we determined an upper limit of branching fraction at 90% confidence, by using Baysian approach.

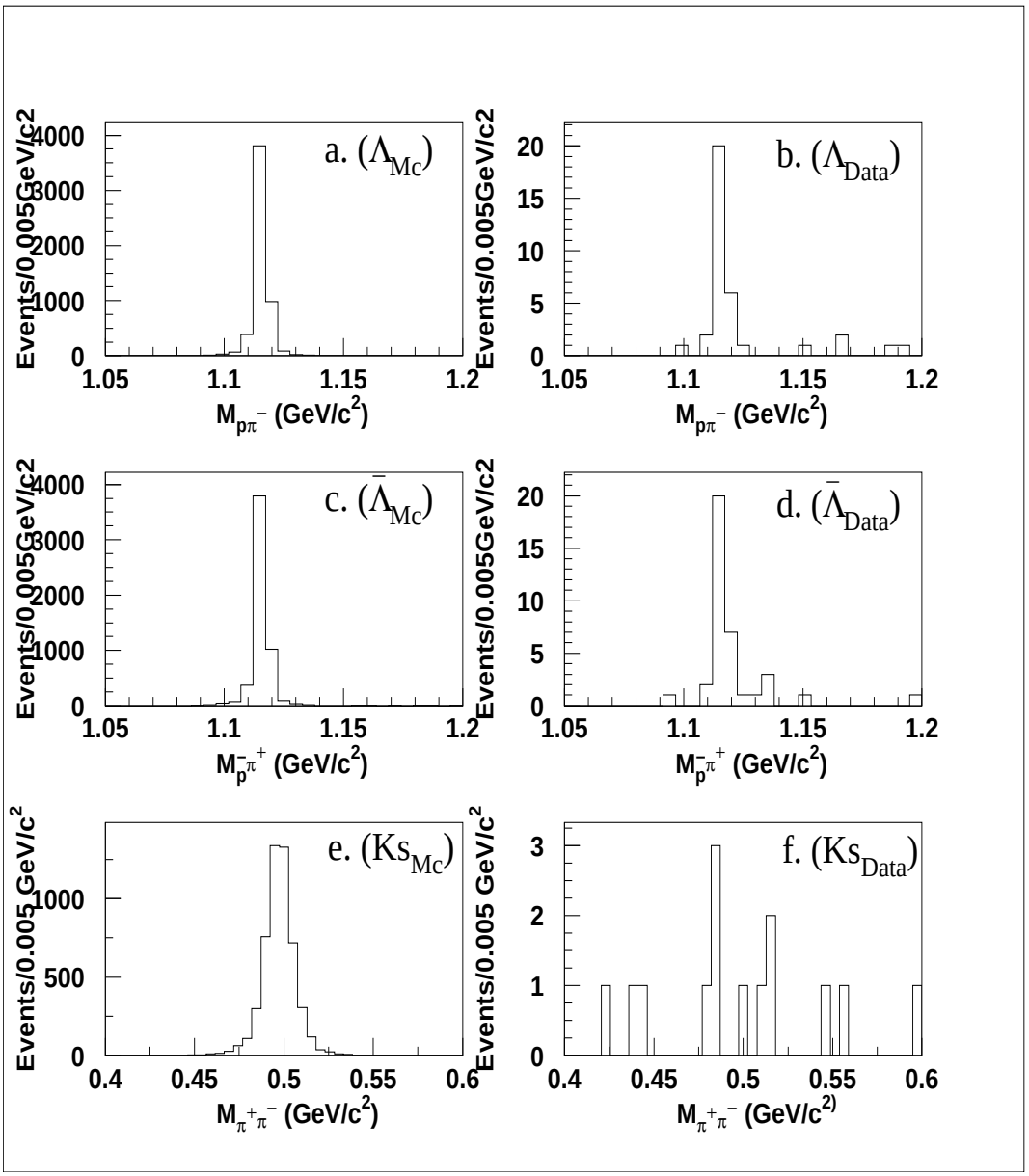

Figure 5.16: The invariant mass distribution of (a) $\Lambda \to p\pi^-(MC)$, (b) $\Lambda \to p\pi^-(data)$, (c) $\bar{\Lambda} \to \bar{p}\pi^+(MC)$, (d) $\bar{\Lambda} \to \bar{p}\pi^+(data)$ (e) $K_s^0 \to \pi^+\pi^-(MC)$, (f) $K_s^0 \to \pi^+\pi^-(data)$ in $\psi(2S) \to \Lambda\bar{\Lambda}K_s^0$ after all cuts [68].

5.12 Fit Results of $M_{\pi^+\pi^-}$

In $\psi(2S) \to \Lambda\bar{\Lambda}K_s^0$ decay channel, we have very clearly found the signals of Λ and $\bar{\Lambda}$ but K_s^0 signal is not obvious. We performed fit to $\pi^+\pi^-$ invariant mass spectrum, taking MC histogram as signal function and Legendre polynomials as background functions. From the fit, we determined the number of events in the signal region. We performed fitting in two different mass ranges: $(0.4-0.6)$ GeV/c^2 and $(0.425-0.575)$ GeV/c^2, using two different background functions - Legendre polynomials of 2nd and 3rd order. Results for 'the maximum likelihood' for $(0.4-0.6)$ GeV/c^2 range with background function of 3rd and 2nd order Legendre polynomials, are shown in Fig. 5.17 and Fig. 5.18, respectively.

According to the result depicted in Fig. 5.17, number of signal events is 1.35 ± 2.8 and the maximum log likelihood is $-2lnL = 28.6$. From fit result of Fig. 5.18, the number of signal events is 1.24 ± 2.9 and maximum log likelihood is $-2lnL = 30.2$. Next, considering the second fit range: $(0.425-0.575)$ GeV/c^2, the results are shown in Fig. 5.19 and Fig. 5.20. Considering both the signal and background contributions from Fig. 5.20, the number of signal events is 1.35 ± 3.32 and maximum log likelihood is $-2lnL = 18.6$. From Fig. 5.19, the number of signal events is 1.30 ± 3.53 and maximum log likelihood is $-2lnL = 18.6$.

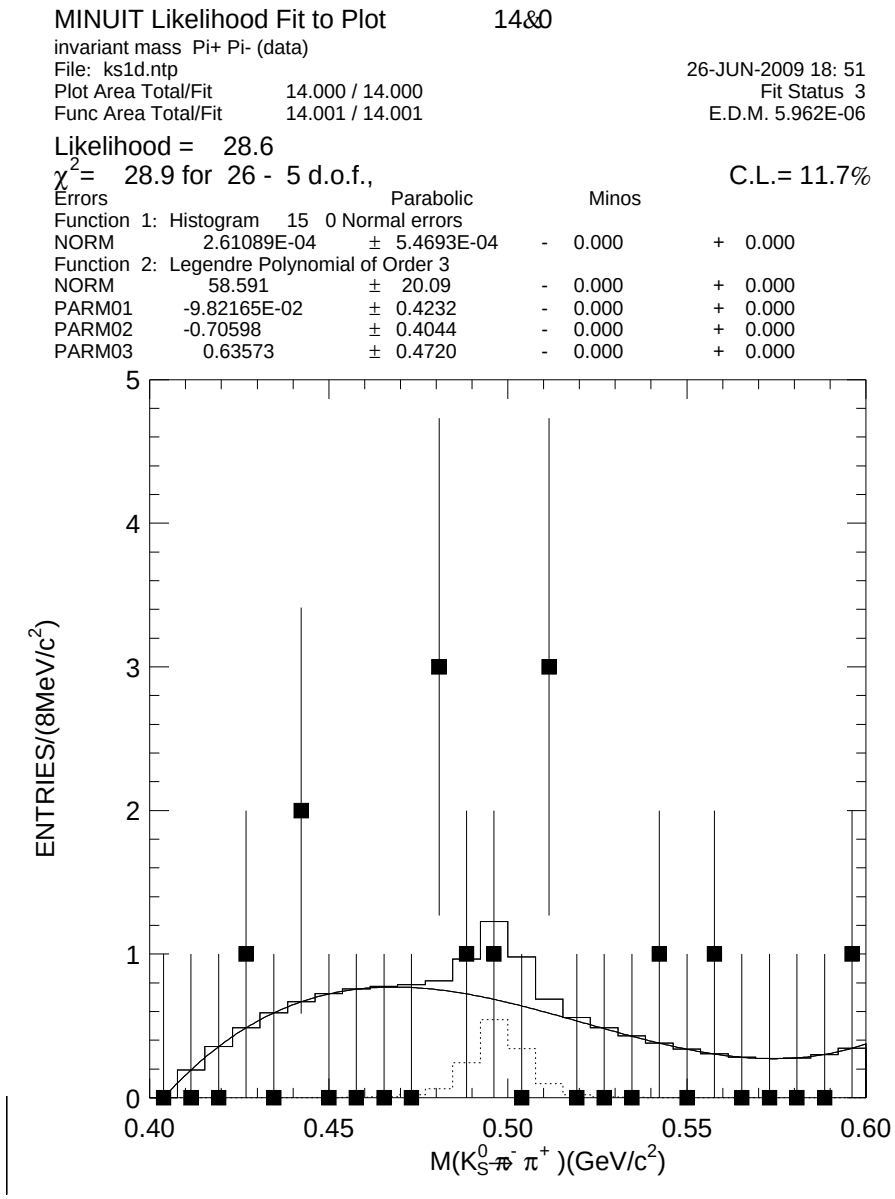

Figure 5.17: Fit result of M($K_s^0 \to \pi^+\pi^-$) with 3rd order Legendre polynomial as background function [68].

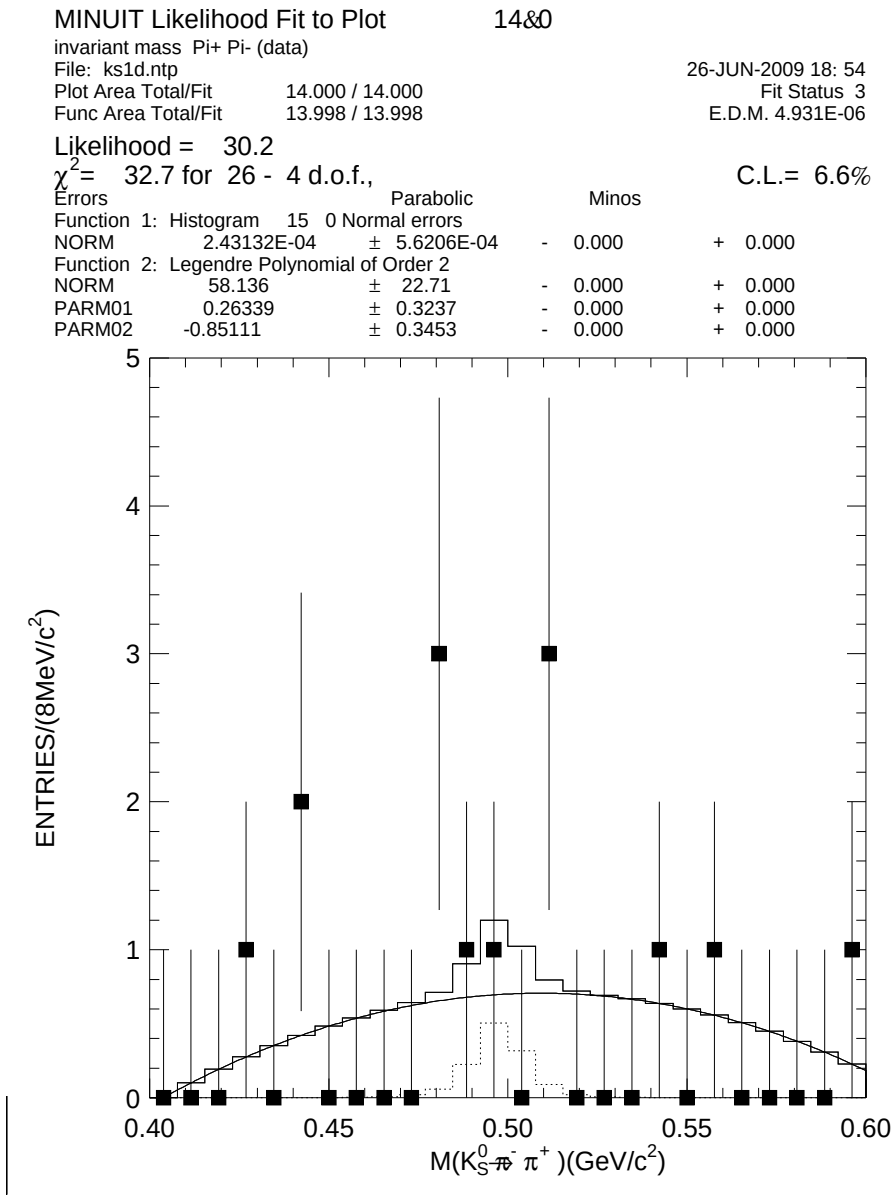

Figure 5.18: Fit result of M($K_s^0 \to \pi^+\pi^-$) with 2nd order Legendre polynomial as background function [68].

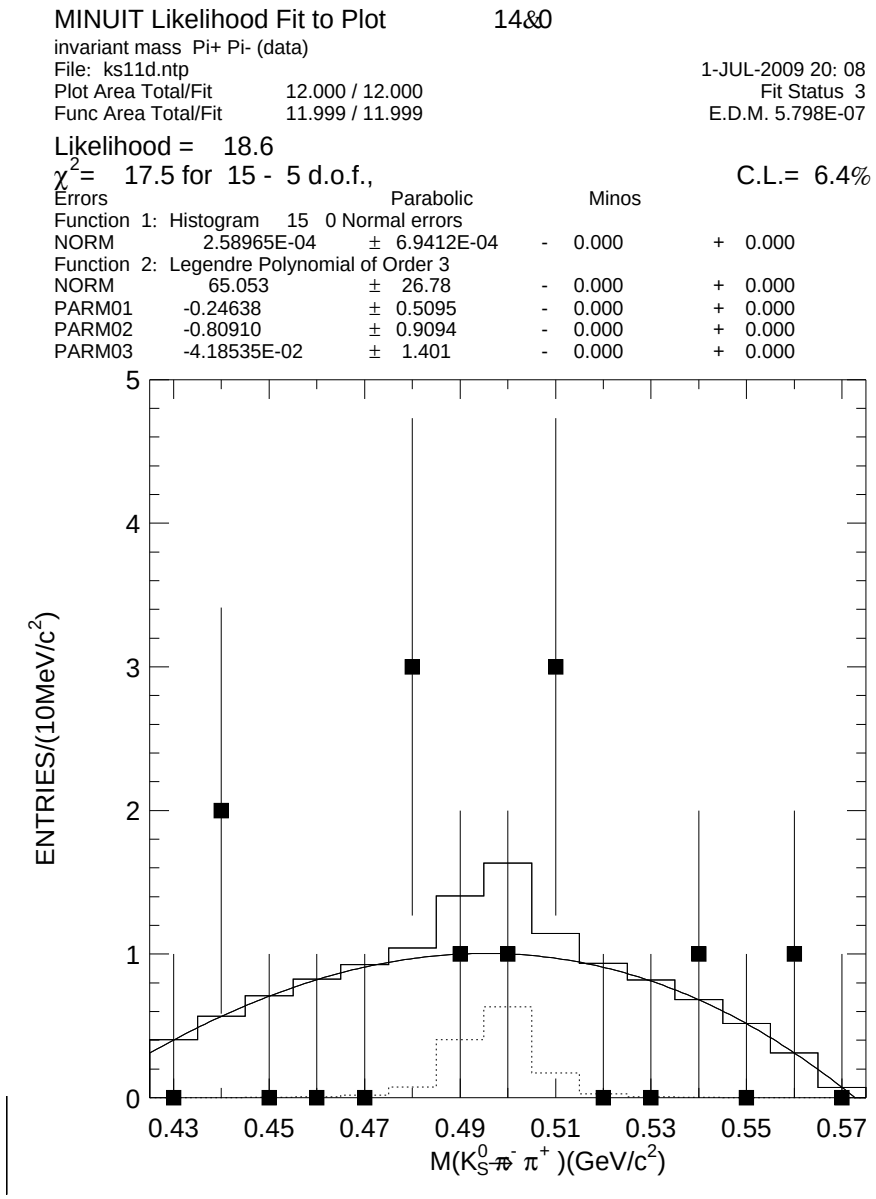

Figure 5.19: Fit result of M($K_s^0 \to \pi^+\pi^-$) with 3rd order Legendre polynomial as background function [68].

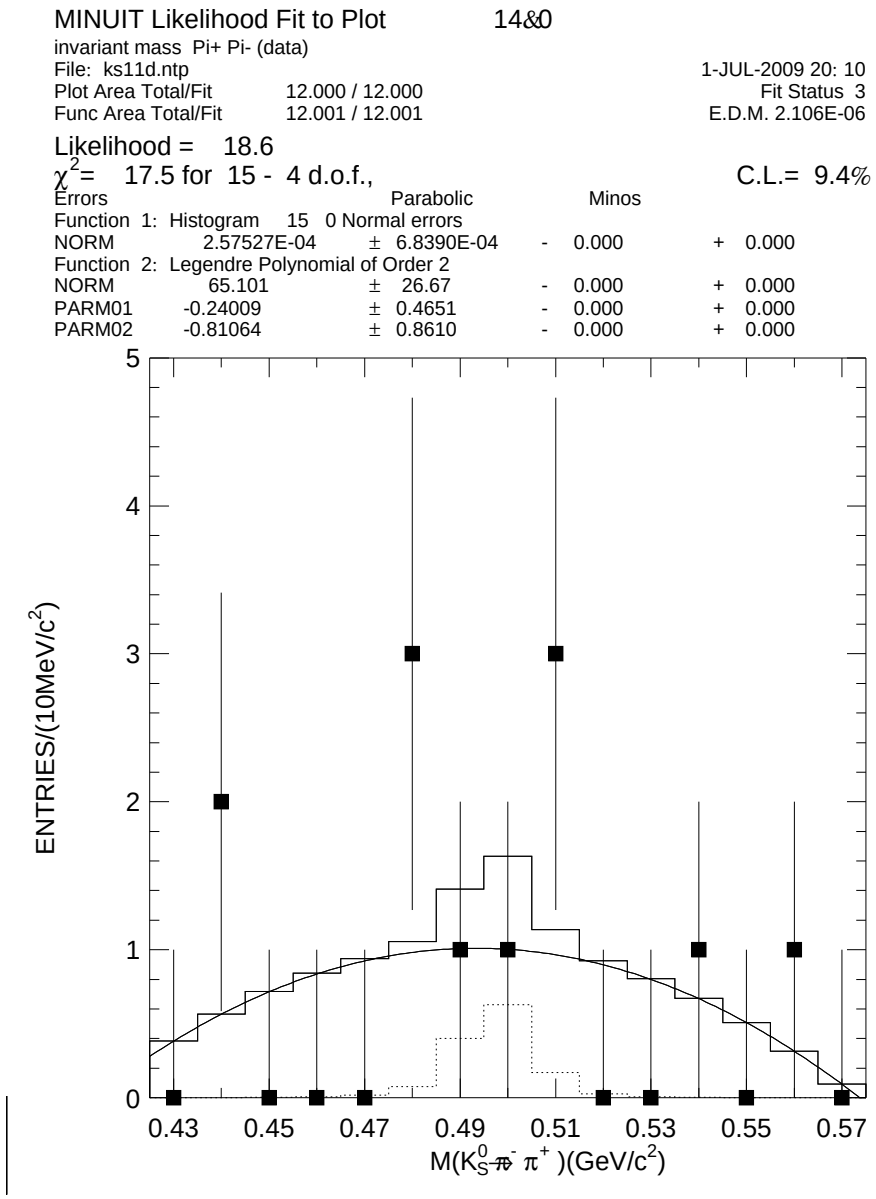

Figure 5.20: Fit result of M($K_s^0 \to \pi^+\pi^-$) with 2nd order Legendre polynomial as background function [68].

5.12.1 Determination of Upper Limit Events

From above four kinds of fit results, it is concluded that there is no clear signal of K_s^0. With the Bayesian approach [71], the upper limit on the number of events at 90% confidence level, was calculated. Fig. 5.21 (a, b, c, d) illustrates the plots for the maximum log likelihood and events. These plots correspond to the Mnfit results shown in Fig. 5.17, 5.18, 5.19 and 5.20. The upper limits on the number of events for K_s^0 are closer to each other, so we take the average number of upper limit numbers, at 90% confidence level, to be 7.5. The results are listed in Tables 5.1 and table 5.2.

5.12.2 Detection Efficiency

For detection efficiency, 2×10^5 MC events were generated using HOWL generator with GCALOR hadronic model. After the final selection criteria, the number of survived events is 5203, with detection efficiency 2.6% [68].

5.13 Systematic errors

Uncertainties in this analysis are mainly from the following sources of error: MDC tracking, Particle Identification (PID), kinematic fit, intermediate branching fractions, K_s^0 reconstruction, Λ and $\bar{\Lambda}$ reconstruction and the $\psi(2S)$ total number. These are described in the following subsections:

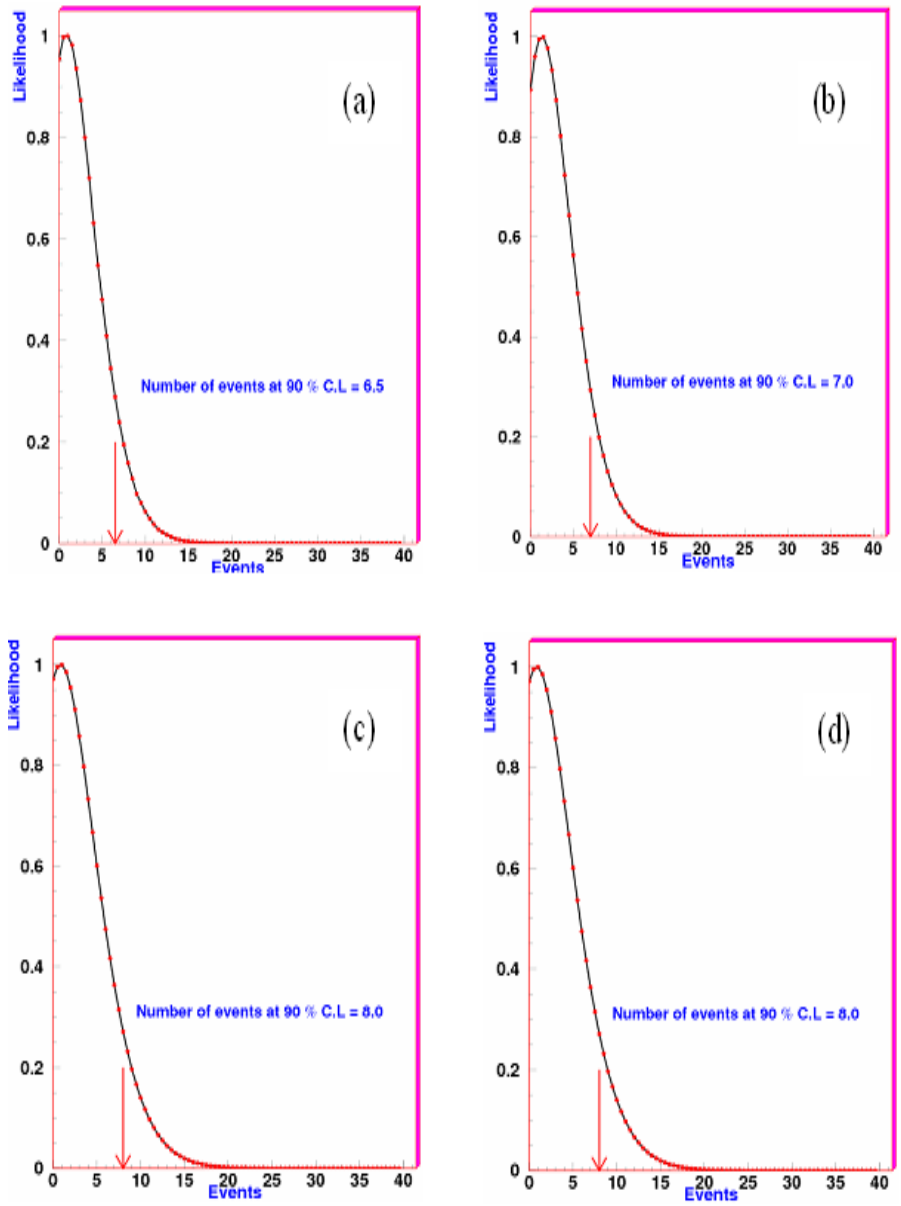

Figure 5.21: Plots (a) and (b) are corresponding to (0.4-0.6)GeV/c^2 mass range with 3rd and 2nd order Legendre polynomial respectively, Plots (c) and (d) are corresponding to (0.425-0.575)GeV/c^2 mass range with 3rd and 2nd order Legendre polynomial respectively [68].

Table 5.1: No. of upper limit events using background of 3rd order Legendre Polynomial [68]

Fit range(GeV/c^2)	No. of upper limit events at 90% C.L.
$0.4 - 0.6$	6.5
$0.425 - 0.575$	8.0

Table 5.2: No. of upper limit events using background of 2rd order Legendre Polynomial [68]

Fit range(GeV/c^2)	No. of upper limit events at 90% C.L.
$0.4 - 0.6$	7.0
$0.425 - 0.575$	8.0

5.13.1 MDC Tracking

Efficiency of MDC tracking has been studied by using decay processes such as $J/\psi \to \Lambda\bar{\Lambda}$, $\psi(2S) \to \pi^+\pi^- J/\psi$ and $J/\psi \to \mu^+\mu^-$. The MC and data tracking efficiencies for each charged track agree within 1 to 2% [40]. In decay of $\psi(2S) \to \Lambda\bar{\Lambda}K_s^0$, 12% is regarded as the error caused by the MDC tracking of six charged tracks.

5.13.2 Particle Identification (PID)

Particle identification efficiency of K, π and p has been studied carefully by BES collaboration [40]. Only one charged track was identified as a proton or an antiproton and the systematic error is less than 2% ($\approx$ 1%). Therefore, 6% was taken as PID error when we account for all the six particles.

5.13.3 MC Model

There are many hadronization models used for simulations of hadronic interactions with detector, each of which gives different detection efficiency. Their differences are taken as the systematic errors. By using the GCALOR [72] and FLUKA [73] models, we generated MC events for determining their efficiencies. We found 14.9% as the MC model error [68].

5.13.4 Kinematic Fit

4C-kinematic fit error is studied by selecting the decay channel $J/\psi \to \Xi^-\bar{\Xi}^+$. We generated 100,000 events using phase space generator. After reconstruction with and without 4C-fit, in data and MC, the relative efficiency difference is 6%.

5.13.5 K_s^0 vertex finding

For the K_s^0 secondary vertex error, we use the channel $J/\psi \to K^{*-}K^+$, where ($K^{*-} \to K_s^0\pi^-$). We found that with and without Klamcorr, the relative efficiency difference is 3.57%. In [74], the efficiency of vertex finding is studied by using $J/\psi \to K^*(892)\bar{K}+$ *c.c.* giving an error of 4.1%.

5.13.6 Λ and $\bar{\Lambda}$ vertex finding

$J/\psi \to \Lambda\bar{\Lambda}$ is chosen to study Λ and $\bar{\Lambda}$ vertex findings error. After reconstruction with and without Klamcorr for data and MC, the relative error was found to be 2.0%. This error was also studied in [75] and the error was determined as 1.2% for each of Λ and $\bar{\Lambda}$.

5.13.7 Intermediate Branching Fractions

The branching fractions of $\Lambda \to p\pi^-$, $\bar{\Lambda} \to \bar{p}\pi^+$ and $K_s^0 \to \pi^+\pi^-$ are taken from PDG [14]. We have taken the errors on these branching fractions as the systematic errors in our measurement. This error is about 1.5%.

Table 5.3: The Systematic Errors for $\psi(2S) \to \Lambda\bar{\Lambda}K_s^0$ [68]

Sources	Relative Error(%)
MDC Tracking	12.0
PID	6.0
MC Model	16.0
Intermediate Decay Br.	1.5
$\psi(2S)$ Number	4.0
Kinematic fit	6.0
Λ reconstruction	2.0
K_s^0 reconstruction	4.0
Total error	21.8

5.13.8 $\psi(2S)$ Total Number

The total number of $\psi(2S)$ events has been determined to be $N_{\psi(2S)} = (14.0 \pm 0.6) \times 10^6$, using inclusive hadronic events [76]. The uncertainty in $\psi(2S)$ events is 4.0% and was taken as systematic error.

The above uncertainties are also listed in table 5.3. The total systematic error is determined to be 21.8%, by adding the individual uncertainties in quadrature.

Chapter 6

Results, Discussion and Conclusions

6.1 Determination of Upper Limit of the Branching Fraction

The upper limit of the branching fraction at 90% confidence level is determined, by using the following relation:

$$B(\psi(2S) \to \Lambda\bar{\Lambda}K_s^0) < \frac{N_{obs}^{UL}}{N_{\psi(2S)}.[B(\Lambda \to p\pi^-)]^2.B(K_s^0 \to \pi^+\pi^-).\epsilon.(1-\sigma_{sys})},$$

where N_{obs}^{UL}, $N_{\psi(2S)}$, ϵ and σ_{sys} represent the upper limit on the observed signal events, total number of $\psi(2S)$ data events, detection efficiency and total systematic error, respectively. Using their values and those of intermediate branching fractions in the above inequality, the upper limit value is evaluated to be $Br(\psi(2S) \to \Lambda\bar{\Lambda}K_s^0) < 9.3 \times 10^{-5}$.

6.2 Significance of Upper Limit for the Branching Fraction

As elaborated in the first chapter and section 5.1, our objective in performing current analysis is 'to probe the probability of isospin and strangeness non-conserving decay process $\psi(2S) \rightarrow \Lambda\bar{\Lambda}K_s^0$'. Keeping in view the importance of our work, we have undertaken an in-depth study of the current decay channel, by including detailed background analysis and maximum possible sources of uncertainties for error analysis. Significance of the upper limit for the branching fraction is highlighted as:

- Before going to set an upper limit on the signal events from data, we have looked for maximum number of background channels from exclusive as well as inclusive MC samples of 14 million $\psi(2S)$ events. After finding the background channels, their contribution in the signal region was subtracted by applying appropriate mass constraints which eliminate the mal-signal contribution of the background channels.

- In order to determine upper limit of signal events in data, we have used Baysean approach. Invariant mass spectra used by this approach were obtained after subtracting the contributions from maximum number of background sources. The upper limit of data events is determined carefully, by considering number of fit ranges and Legendre's polynomials of different orders as background functions. The upper limit numbers (6.5, 7.0, 8.0, 8.0) on the data events thus obtained

were found to be with an uncertainty of (13-20)% from their average is 7.5.

- As described above, in addition to detailed background analysis and careful determination of upper limit of signal data events, we have considered large number of uncertainty sources to approximate total systematic uncertainty. Total uncertainty value thus obtained has been used in the formula meant for setting an upper limit for the branching fraction of $\psi(2S) \to \Lambda\bar{\Lambda}K_s^0$.

From the above highlights, we report that the upper limit for the branching fraction has been determined very carefully. After detailed consideration of almost all aspects of analysis, it is found that the upper limit result (9.3×10^{-5}) is not so small.

6.3 Future Perspective for the Branching Fraction Result

In the light of our analysis for the upper limit of $\psi(2S) \to \Lambda\bar{\Lambda}K_s^0$, the following conclusions are drawn. In doing so we have also taken in to account the future perspective at BES III with the availability of the huge amount of data for further analysis. We thus conclude:

- In this work we could only report an upper limit for the branching fraction of $\psi(2S) \to \Lambda\bar{\Lambda}K_s^0$ due to paucity of event/data. A relatively large value of upper limit ($9.3 \times 10^{-5} \sim 10^{-4}$) which can not be ignored indicates the significant probability of occurrence of the signal channel when more data will be available

at BES III. Our upper limit result is therefore of prime importance as it would provide an evidence or observation of current decay process which may lead to new physics on charmonium decays. As shown in Fig 4.3, strangeness and isospin non-conserving decay mode, if observed, will open a new chapter of weak interaction of charmonium states below $D\bar{D}$ threshold. Importance of this study can be further understood in the sense that it indicates significant chances ($\sim 10^{-4}$) of isospin and strangeness non-conserving mode.

- Upper limit result demands further investigation by using large statistics of $\psi(2S)$ data. In this direction, BESIII has recorded a huge samples of J/ψ as well as $\psi(2S)$ so far. At the time of writing of this thesis, BESIII has already reported 100 million of J/ψ and about 200 million $\psi(2S)$ data events. Data samples of J/ψ and $\psi(2S)$ are expected to grow further in the near future. Huge sample of $\psi(2S)$ data events will be of immense importance.

- However, if the current decay mode is not observed when the BES III data is fully available for analysis, it will further enhance the credibility of the standard model. Any evidence or observation will provide a hint beyond the standard model. An observation of the current decay process will indicate that charmonium state $\psi(2S)$ can decay through strong interaction followed by weak interaction involved at gluonic level as depicted in Fig. 4.3.

- Systematic error for the branching fraction of the current decay processes will

be investigated precisely by using better BESIII analysis tools such as MC event generators, GEANT4 (a detector simulation toolkit), event reconstruction software, etc.

Bibliography

[1] Robert N. Cahn, Gerson Goldhaber, The Experimental foundations of Particle Physics, 2nd edition, Cambridge University, London, 2009.

[2] W. N. Cottingham and D. A. Greenwood, Introduction to the standrad model of particle physics, Cambridge University, London, 2007.

[3] Donald H.Perkins, Introduction to high energy physics, Cambridge University, London, 2000.

[4] B.R. Martin and G. Shaw. Particle Physics. John Wiley and Sons, second edition edition, 1997.

[5] James William Rohlf, Modern physics from α to $z0$, John Wiley and Sons,NewYork, 1994.

[6] BES Collaboration, J. Z. Bai et al., Phys. Lett. B 424,213 (1998).

[7] BES Collaboration, M. Ablikim, et al., Phys. Rev. D 76, 092003, (2007).

[8] P. Henrard et al. DM2 Collaboration, Nucl. Phys. B 292, 670 (1987).

[9] D. Griffiths, Introductory Elementary Particles, Harper and Row Pub., New York, (1987).

[10] Retrieved from "$http://en.wikipedia.org/wiki/Plumpuddingmodel$".

[11] Fayyazuddin and Riazuddin, A modern introduction to particle physics, McGraw-Hill, London, 1992.

[12] I.S. Hughes, Elementary Particles, 3rd Ed., Cambridge Univ. Press, Cambridge, (1990)

[13] Francis Halzen and Alan D. Martin, Quarks and leptons, John Wiley, New York,1984.

[14] W.M.Yao, et al., Particle Data Group, Journal of Physics G 33, 1 (2006) and 2007 particle update for the 2008 edition.

[15] M. Gell-Mann and Y. Neeman, The eightfold way, Benjamin, New York, 1964.

[16] J. J. Kokkedee, The quark model, Benjamin, New York, 1969.

[17] V. Barnes et al, Phys. Rev. Lett. 12 (1964), 204.

[18] Gell-Mann and Murray, The quark and the jaguar, Owl Books,1995.

[19] Mikhail A.; Ericson T.; Landshof P. Y Kogut, John B.; Stephanov, From confinement to extreme environments, Cambridge University Press, 2003.

[20] Schafer Andreas Greiner, Walter, Quantum chromodynamics, Springer, 1994.

[21] A.W. Hendry and D.B. Lichtenberg, Rep. Prog. Phys. 41 (1978), 1707.

[22] M. H.Ye et al. IHEP project report of BES at BEPC. In M.Riordan, editor, 1989 Int. Symp. on Lepton and Photon Interactions at High Energies, page 122. Stanford, 1989.

[23] Y.Wu.,Operational status and future upgrades of the BEPC,Talk given at the 18th Particle Accelerator Conference. (1999).

[24] D. Bernstein et al., Nucl. Instr. Methods 226, 301 (1984) and the references therein.

[25] N. Brambilla et al. Heavy Quarkonium Physics. CERN Yellow Report, 2005. QWG and Topic conveners.

[26] Retrieved from *http://www.ihep.ac.cn/english/E-Bepc/index.htm*

[27] X.H.Mo et al., Determination of $\psi(2S)$ total number by inclusive hadronic decay, High Energy Phys. and Nucl. Phys.,**27**,(2004), 455.

[28] BESII publications Book 2004-2008, complied by Institute of High Energy Physics, Yuquan Lu Beijing, Chia.

[29] BES Collaboration, J.Z. Bai, et al., Nucl. Instrum. Methods A 344 (1994) 319.

[30] BES Collaboration, J.Z. Bai, et al., Nucl. Instrum. Methods A 458 (2001) 627.

[31] T. Yamamura, *Study of J/ψ Meson Decaying into Baryon-Antibaryon Final States with the BES-II Detector*, PhD thesis, university of Tokyo, 2007.

[32] M. H.Ye et al., High Energy Phys. and Nucl. Phys. 28, (2004) 1135.

[33] J.M.Ma et al., High Energy Physics and Nucl. Phys.14, (1990)325.

[34] H.J.Bhabha. The Scattering on Positrons by Electrons with Exchange on Dirac's Theory of the Positron. Proc. Roy. Soc., A 154 (1936) 195.

[35] Y.H.Zhou et al.,High Energy Physics and Nucl. Phys. 14, (1990)105.

[36] Jin Li et al.,High Energy Physics and Nucl. Phys. 15, (1991) 101.

[37] Y.S.Zhu et al.,High Energy Physics and Nucl. Phys. 14 (1990) 1.

[38] H.L.Ni et al.,High Energy Physics and Nucl. Phys. 14 (1990) 237.

[39] C.Jiangchuan et al.,"Summary of SIMBES Development",(BES note) (2002).

[40] BES Collaboration, M. Ablikim, et al., Nucl. Instrum. Methods A 55 (2005) 344.

[41] R.Brun et al., "GEANT3.21", CERN Report No.DD/EE/84-1 (1987).

[42] Agnes Lundborg, The charm of excited glue, digital comprehensive summaries of uppsala dessertations from faculty of science and technology 269.

[43] Prof. Korytov., Lecture notes, retrieved from:*http://www.phys.ufl.edu/korytov/phz6355/note-A21-cbt-generation-count.pdf*

[44] Diego Bettoni, Roberto Calabrese, Review Charmonium spectroscopy, Progress in Particle and Nuclear Physics 54 (2005) 615651.

[45] J.J. Aubert et al., Experimental observation of a heavy particle j, Phys. Rev.Lett. 33(1974), 1404.

[46] J.-E Augustin et al., Discovery of a narrow resonance in e-e+ annihilation., Phys. Rev. Lett. 33 (1974), 1406.

[47] S.Okubo, Phys. Lett. 5, 165 (1963)

[48] G. Zewig, CERN-preprints CERN-TH-401,402,412 (1964)

[49] J. Iizuka, Prog. Theor. Phys. Suppl. 37-38, 21 (1966)

[50] L.Kopke and N.Wermes, Physics Report 174(1989)67-227.

[51] R. Sinha and S. Okubo, Phys. Rev. D30, 2333(1984).

[52] C. Bacci et al., Preliminary result of frascati (adone) on the nature of a new 3.1 GeV particle produced in e^-e^+ annihilation., Phys. Rev. Lett. 33 (1974), 1408.

[53] G.S. Abrams et al., Discovery of a second narrow resonance in e-e+ annihilation.,Phys. Rev. Lett. 33 (1974), 1453.

[54] B. Richter, From the psi to charm: the experiments of 1975 and 1976, Rev. Mod. Phys. 44 (2)(1977), 251.

[55] Cleo results rerieved from:*https://wiki.lepp.cornell.edu/lepp/bin/view /CLEO/PublicResults.*

[56] H.J. Besch et al, phy. Lett. B 78 (1978), 347.

[57] H.J. Besch et al, Zeit. Phy. C 8(1981).

[58] I. Peruzzi et al, phy. Rev. D 17 (1978), 2901.

[59] R.Brandelik et al, Z. Phy. C1 (1979), 233.

[60] M.W.Eaton et al., Phys. Rev. D29, 804 (1984).

[61] P.Henrard et al., Nucl. Phys. B 292 (1987) 670-692.

[62] D. Pallin et al, Nucl. Phy. B 292 (1987), 653.

[63] J.S. Brown, Phd thesis, univ. of washington, vol. UMI 84-19117-mc, unpublished, 1984.

[64] M. J. Gibb et al. Monte Carlo Simulation of Baryon and Lepton Number Violating Processes at High Energies, CERN-TH.7090/93, Cavendish-HEP-93/6.

[65] J. A. Formaggio et al. Search for the Lepton Family Number Violating Process, Phys. Rev.Lett. 87 (2001).

[66] BES Collaboration, M.Abilkim, et al., Phys. lett. B 598,(2004) 172-177.

[67] El. Hassan Kada et al Z-Phys, C70(1996) 303-306 (and the references therein).

[68] Analysis Memo based upon *Search for* $\Psi(2S) \to \Lambda\bar{\Lambda}K_s^0$, has been finalized by BES Collaboration and is being submitted for publication, 2009.

[69] BES Collaboration, M. Ablikim, et al.,Phys.Lett. B 659 789-795, (2008).

[70] J. C. Chen et al., Phys. Rev. D62 (2000) 034003.

[71] Andrew D. Martin "The Oxford Handbook of Political Methodology" chapter no.21, Beysian Analysis.

[72] C. Zeitnitz and T.A. Gabriel, Nucl. Instr. and Meth. A 349 (1994) 106. (1992) 412.

[73] A. Ferrari, P.R. Sala, G. Guaraldi and F. Padoani, Nucl. Instr. Meth. B 71 (1992) 412.

[74] BES Collaboration, M. Ablikim, et al.,Phys.Rev.Lett. 92, 052001,(2004).

[75] BES Collaboration, M. Ablikim, et al.,Phys.Lett. B 648,149,(2007).

[76] X. H. Mo et al.,HEP and NP, 28, 455, (2004).